



Deposited via The University of Leeds.

White Rose Research Online URL for this paper:

<https://eprints.whiterose.ac.uk/id/eprint/169827/>

Version: Accepted Version

Article:

Wei, Y, Wang, C, Liu, X et al. (2020) Impact of microfluidization and thermal treatment on the structure, stability and in vitro digestion of curcumin loaded zein-propylene glycol alginate complex nanoparticles. Food Research International, 138 (Part B). 109817. ISSN: 0963-9969

<https://doi.org/10.1016/j.foodres.2020.109817>

© 2020, Elsevier Ltd. This manuscript version is made available under the CC-BY-NC-ND 4.0 license <http://creativecommons.org/licenses/by-nc-nd/4.0/>.

Reuse

This article is distributed under the terms of the Creative Commons Attribution-NonCommercial-NoDerivs (CC BY-NC-ND) licence. This licence only allows you to download this work and share it with others as long as you credit the authors, but you can't change the article in any way or use it commercially. More information and the full terms of the licence here: <https://creativecommons.org/licenses/>

Takedown

If you consider content in White Rose Research Online to be in breach of UK law, please notify us by emailing eprints@whiterose.ac.uk including the URL of the record and the reason for the withdrawal request.

1 *Impact of microfluidization and thermal treatment on the structure, stability and in*
2
3 *vitro digestion of curcumin loaded zein-propylene glycol alginate complex*
4
5
6 *nanoparticles*
7
8

9
10 Yang Wei^{a, b}, Chao Wang^a, Xin Liu^a, Alan Mackie^b, Liang Zhang^a, Jinfang Liu^a, Like

11
12
13 Mao^a, Fang Yuan^a, Yanxiang Gao^{a*}
14

15
16 ^a*Beijing Advanced Innovation Center for Food Nutrition and Human Health,*
17
18 *Beijing Laboratory for Food Quality and Safety, Beijing Key Laboratory of*
19
20 *Functional Food from Plant Resources, College of Food Science & Nutritional*
21
22 *Engineering, China Agricultural University, Beijing, 100083, P. R. China*
23
24

25
26
27 ^b*Food Colloids and Processing Group, School of Food Science and Nutrition,*
28

29
30 *University of Leeds, Leeds LS2 9JT, UK*
31
32
33
34
35
36
37
38
39
40
41
42
43
44
45
46

47 *Corresponding author.

48
49 Tel.: + 86-10-62737034

50
51 Fax: + 86-10-62737986

52
53
54 Address: Box 112, No.17 Qinghua East Road, Haidian District, Beijing 100083,
55
56
57 China

1
2
3
4
5
6
7
8
9
10
11
12
13
14
15
16
17
18
19
20
21
22
23
24
25
26
27
28
29
30
31
32
33
34
35
36
37
38
39
40
41
42
43
44
45
46
47
48
49
50
51
52
53
54
55
56
57
58
59
60
61
62
63
64
65

1 **Abstract:**

2 The aim of this study was to modulate the physicochemical properties, molecular
3 interactions and microstructure of zein-propylene glycol alginate (PGA) complex
4 nanoparticles for delivery of curcumin with the aid of high pressure microfluidization
5 (HPM) (50-150 MPa) and thermal treatment (45-85 °C). The size of zein-PGA complex
6 nanoparticles was decreased to around 300 nm. It was confirmed that the pressure of
7 100 MPa and temperature of 75 °C were the optimum parameters to provide a better
8 protection of entrapped curcumin against environmental stresses. The electrostatic
9 interaction, hydrogen bonding and hydrophobic attraction were the dominant driving
10 forces in the formation of the complex nanoparticles. Field emission scanning electron
11 microscopy (FE-SEM) revealed that HPM and thermal treatment facilitated the
12 complex nanoparticles to form a more uniform size and spherical shape. During *in vitro*
13 gastrointestinal digestion, zein-PGA complex nanoparticles showed excellent gastric
14 stability and sustained-release of curcumin in the small intestine. HPM and thermal
15 treatment showed a synergistic effect on enhancing the bioaccessibility of curcumin
16 entrapped in zein-PGA complex nanoparticles. The findings revealed the influence of
17 HPM and thermal treatment on functional attributes of the complex nanoparticles,
18 which could be utilized to design food grade nanoparticles with desirable stability and
19 digestive properties.

20 **Key words:** Zein-PGA complex nanoparticles; Curcumin; High-pressure
21 microfluidization; Thermal treatment; Physicochemical stability; *In vitro* digestion
22

24 1. Introduction

25 Food nanoparticles have gained considerable attention due to their beneficial
26 characteristics including biocompatibility, biodegradability, and mucoadhesive ability,
27 which can be utilized to deliver bioactives through improving water solubility, chemical
28 stability and bioavailability (Semenova, 2017). Proteins are the most important
29 biomaterials to produce food nanoparticles, which are regarded as environmentally
30 sustainable with high nutritional values. Nevertheless, the protein-based colloids
31 usually lose their structural stability when the physiological pH is close to isoelectric
32 point (pI) or under extreme stresses (heat, high pressure or salts). Most of proteins can
33 be digested by proteases in the stomach and the bioactives entrapped would be released
34 (McClements & Gumus, 2016). To improve the stability of nanocarriers,
35 polysaccharides are usually introduced to coat the protein particles as a shell or interact
36 with proteins to fabricate stable hybrid nanoparticles (Huang et al., 2017; Joye,
37 Davidov-Pardo, & McClements, 2015). The presence of polysaccharides provides the
38 steric and electrostatic repulsion among the colloidal particles, preventing aggregation
39 and sedimentation and modulating the release and adsorption of nutraceuticals loaded
40 during gastrointestinal digestion.

41 The modification of proteins to broaden their application has been widely reported,
42 such as induction of heat, high pressure, enzymes and ionic gelation. High pressure
43 processing and thermal treatment are the most important strategies to modulate the
44 properties of biopolymers, which are widely utilized in industrial applications. High

1 45 pressure microfluidization (HPM) has been utilized to modulate the functional
2
3 46 attributes of various water-soluble proteins, including whey protein (Dissanayake &
4
5
6 47 Vasiljevic, 2009), peanut protein (Hu, Zhao, Sun, Zhao, & Ren, 2011), and soy protein
7
8
9 48 (Song, Zhou, Fu, Chen, & Wu, 2013). Besides, researchers reported that thermal
10
11
12 49 processing was utilized to modify structural properties of alcohol-soluble proteins
13
14
15 50 (zein). Zein is a plant protein extracted from corn, which is a promising biomaterial for
16
17
18 51 several industrial applications (Paliwal & Palakurthi, 2014). As reported by previous
19
20
21 52 researchers, zein can be well dissolved in 50%-90% (v/v) aqueous ethanol solutions
22
23
24 53 (Shukla & Cheryan, 2001). It can be self-assembled into films, fibers, microspheres and
25
26
27 54 nanoparticles due to its highly hydrophobic amino acid proportion (Momany et al.,
28
29
30 55 2006; Shukla & Cheryan, 2001; Wei, Sun, Dai, Zhan, & Gao, 2018; Wei, Yu, et al.,
31
32
33 56 2020). Propylene glycol alginate (PGA) is a kind of polysaccharide with surface-
34
35
36 57 activity attributed to its propylene glycol groups, which can interact with zein to form
37
38
39 58 the stable complexes for delivery of **bioactives** (Wei, Yu, et al., 2019).

40
41
42 59 Most of the previous efforts on adjusting the molecular structure of zein to improve
43
44
45 60 its functional properties focused on adjusting the degree of protein aggregation,
46
47
48 61 structure, and rheological properties through adjusting the ethanol concentration and
49
50
51 62 pH of the solvent where the prolamin was dissolved (Kim & Xu, 2008; Selling,
52
53
54 63 Hamaker, & Sessa, 2007; Zhang, Luo, & Wang, 2011). Additionally, they investigated
55
56
57 64 the influence of temperature on the conformation of zein and found that the alteration
58
59
60 65 of zein structure mainly occurred at **70 °C** (Selling et al., 2007). Microfluidization could
61
62
63 also be incorporated into the protein modification, which influenced the hydrogen
64
65

1 67 bonding and hydrophobic interactions among the protein-protein or protein-
2
3 68 polysaccharide complexes through high pressure, shear stress, turbulence and
4
5
6 69 cavitation (Ye & Harte, 2014). Based on a previous work, the combined thermal
7
8
9 70 treatment with HPM was confirmed to alter the physicochemical and conformational
10
11
12 71 properties of zein (Sun, Dai, Liu, & Gao, 2016). Nevertheless, there is no information
13
14
15 72 available about the influence of the coupled treatments of heating and HPM on the
16
17
18 73 functional attributes, environmental stability and *in vitro* digestion of protein-
19
20
21 74 polysaccharide binary complex nanoparticles for delivery of nutraceuticals. The
22
23
24 75 objective of this study was to investigate the potential of heating and HPM applied in
25
26
27 76 the development of nanoparticle-based delivery vehicles.

28
29 77 In this study, curcumin was chosen as a model polyphenolic compound to be
30
31
32 78 encapsulated into the zein-PGA complex nanoparticles through the emulsification-
33
34
35 79 evaporation method. Different microfluidization pressures (50-150 MPa) and heating
36
37
38 80 temperatures (45-85 °C) were utilized to modulate the physicochemical, conformational
39
40
41 81 and morphological properties of the complex nanoparticles. The stability of complex
42
43
44 82 nanoparticles was assessed systematically under various environmental stresses (light,
45
46
47 83 heat, pH and salts). The conformational alteration, secondary structure of zein,
48
49
50 84 intermolecular interactions and thermal behavior were analyzed to reveal the formation
51
52
53 85 mechanism of the complex nanoparticles. The **release percentage** and bioaccessibility
54
55
56 86 of curcumin loaded in complex nanoparticles were appraised during the simulated
57
58
59 87 gastrointestinal (GI) tract.

60
61
62
63
64
65
66 88

89 2. Materials and methods

90 2.1. Materials

91 Zein (CAS: 9010-66-6) with a protein content of 91.3%, pepsin (pack size: P7012),
92 pancreatin (pack size: P1750) and bile salts (pack size: 48305) were purchased from
93 Sigma-Aldrich (St. Louis, MO, USA). It has been reported that pepsin activity was
94 greater than 2500 units/mg protein. The bile salts were composed of 50% deoxycholic
95 acid sodium salt and 50% cholic acid sodium salt. Propylene glycol alginate (PGA)
96 (CAS: 9005-37-2) (esterification: 87.9%) was kindly provided by Hanjun Sugar
97 Industry Co. Ltd. (Shanghai, China). Curcumin (>98%) (CAS: 458-37-7) was obtained
98 from Adamas-Beta (Shanghai, China). Absolute ethanol (99.99%), solid sodium
99 hydroxide and liquid hydrochloric acid (36%, w/w) were acquired from Eshowbokoo
100 Biological Technology Co., Ltd. (Beijing, China).

101

102 2.2. Preparation of curcumin loaded zein-PGA complex nanoparticles

103 Briefly, 0.60 g of zein, 0.30 g of PGA and 0.10 g of curcumin were added into 160
104 mL 70% (v/v) aqueous ethanol solution in sequence to form the mixed solution with
105 magnetic stirring under 600 rpm at 25 °C until their complete dissolution.

106 To investigate the influence of HPM pressure on the attributes of curcumin loaded
107 zein-PGA binary complexes, the mixed solutions were subjected to microfluidization
108 at 50, 75, 100, 125 and 150 MPa for 2 cycles at 25 °C by a Microfluidizer® processor
109 model M-110EH (Microfluidics, Newton, MA, USA) (Sun, Dai, Liu, et al., 2016). All
110 the solutions were then evaporated at 45 °C for 40 min to remove the ethanol and the

1 111 remaining volume was set to around 40 mL, which was then diluted with distilled water
2
3 112 (pH 4.0) to 100 mL. The particle suspensions were centrifuged (Sigma 3k15, DJB
4
5
6 113 labcare, Buckinghamshire, UK) at $725 \times g$ for 10 min to remove large particle
7
8
9 114 aggregates and untrapped curcumin. The supernatants were collected. Thereafter,
10
11 115 part of samples was placed at 5 °C for further analysis and the other part was freeze-
12
13 116 dried for 48 h to obtain powder samples. The samples were termed as ZP-50MPa, ZP-
14
15 117 75MPa, ZP-100MPa, ZP-125MPa and ZP-150MPa, respectively.
16
17
18
19

20 118 To investigate the influence of thermal treatment and HPM pressure on the
21
22 119 properties of curcumin loaded zein-PGA binary complexes, the mixed solutions (0.60
23
24 120 g of zein, 0.30 g of PGA and 0.10 g of curcumin in 160 mL 70% (v/v) aqueous ethanol)
25
26 121 were placed in a thermostatic water bath for 30 min at 45, 55, 65, 75 and 85 °C.
27
28 122 Thereafter, the solutions were subjected to microfluidization at 100 MPa for 2 cycles
29
30 123 immediately. The following procedure of the nanoparticle dispersions was performed
31
32 124 as the aforementioned process. The samples were termed as ZP-45°C, 100MPa, ZP-55°C,
33
34 125 100MPa, ZP-65°C, 100MPa, ZP-75°C, 100MPa and ZP-85°C, 100MPa.
35
36
37
38
39
40
41

42 126 As the controls, zein nanoparticles, zein nanoparticles with the combined
43
44 127 microfluidization and thermal treatment, curcumin loaded zein nanoparticles, curcumin
45
46 128 loaded zein nanoparticles with the combined microfluidization and thermal treatment
47
48 129 and curcumin loaded zein-PGA complex nanoparticles without any processing were
49
50 130 prepared by following the same procedure as aforementioned, which were termed as Z,
51
52 131 Z-75°C,100MPa, Z-cur, Z-cur-75°C,100MPa and ZP, respectively. Besides, the samples
53
54 132 with individual heating (75 °C, 0MPa) and HPM (25 °C, 100 MPa) processing were
55
56
57
58
59
60
61
62
63
64
65

1 133 prepared and named as ZP-75°C and ZP-100MPa.

2
3 134

4
5 135 *2.3. Particle size distribution and zeta-potential*

6
7 136 Particle size and zeta-potential of the particle dispersions were determined by using
8
9 137 a Nano-ZS90 (Zetasizer, Malvern Instruments Ltd., Worcestershire, UK). Stokes-
10
11 138 Einstein equation and Smoluchowski model were used in the calculation of particle size
12
13 139 and zeta potential, respectively. The samples were diluted 10 times with pH-adjusted
14
15 140 distilled water (pH 4.0) to avoid multiple light-scattering effect. The type of cuvette
16
17 141 used was DTS1060 and the scattering angle was 90°. The refractive index (RI) of water
18
19 142 was set as 1.45 and the RI of the complex nanoparticles was set as 1.52. All the
20
21 143 measurements were carried out at 25 °C in triplicate.
22
23
24
25
26

27 144

28
29
30 145 *2.4. Encapsulation efficiency and loading capacity*

31
32
33 146 The content of curcumin entrapped in the complex nanoparticles was determined
34
35 147 by following our previous method (Dai, Wei, et al., 2018a). Briefly, 1 mL of freshly
36
37 148 prepared particle dispersions was mixed with 4 mL ethanol through vortex oscillation
38
39 149 for 2 min. Each sample was centrifuged at a speed of 10,000 × g for 30 min and the
40
41 150 supernatant was collected. Thereafter, the curcumin in the supernatant was diluted to
42
43 151 an appropriate concentration (0-6 µg/mL) with 80% aqueous ethanol solution (v/v).
44
45 152 Absorbance was measured with a UV-1800 spectrophotometer (Shimadzu Corporation,
46
47 153 Kyoto, Japan) at 426 nm. The concentration of curcumin was obtained by referring to
48
49 154 a standard curve ($R^2=0.999$) of curcumin prepared under the same condition.
50
51
52
53
54
55
56

57
58 155 Encapsulation efficiency (EE) and loading capacity (LC) were calculated by
59
60

156 following equations 1 and 2 below:

$$157 \quad EE (\%) = \frac{\text{entrapped curcumin (mg)}}{\text{total curcumin input (mg)}} \times 100 \quad (1)$$

$$158 \quad LC (\%) = \frac{\text{entrapped curcumin (mg)}}{\text{total weight of zein,PGA,TS and curcumin input (mg)}} \times 100 \quad (2)$$

159 Entrapped curcumin means the total content of curcumin encapsulated into the
160 complex nanoparticles. Total curcumin input means the total content of curcumin used
161 during preparation of the nanoparticles.

163 2.5. Physicochemical stability

164 2.5.1. Physical stability

165 The physical stability of all the particle dispersions was estimated with the
166 LUMiSizer (LUM GmbH, Berlin, Germany) based on the principle that the
167 centrifugation accelerates the instability phenomenon (Sobisch & Lerche, 2008). The
168 parameters used in the measurement were adapted as follows: 1.8 mL of colloidal
169 dispersion; rotational speed, 3000 rpm; performed time, 3600 s; time interval, 20 s;
170 temperature, 25 °C.

171 2.5.2. Photostability

172 The photostability of curcumin in the complex particles against UV photolysis was
173 tested. Briefly, 20 mL of freshly prepared complex particles was placed into transparent
174 glass vial. Then samples were put into a controlled light cabinet (Q-Sun, Q-Lab
175 Corporation, Ohio, USA) for up to 2 h under the exposing light condition (40 °C, 0.35
176 W/m²) (Wei, Yu, et al., 2019). The remaining curcumin was determined as described in
177 section 2.4. The retention rate of curcumin was plotted against time.

1 178 *2.5.3. Thermal stability*

2
3 179 Briefly, 5 mL of freshly prepared curcumin loaded complex particles was placed
4
5
6 180 into transparent glass vial and incubated in water bath at 85 °C for 30 min and then
7
8
9 181 cooled down to 25 °C (Wei et al., 2018). The retention rate of curcumin was measured
10
11 182 as described in section 2.4.

13
14 183 *2.5.4. pH stability*

15
16
17 184 Freshly prepared particle dispersions were adjusted to pH 2, 6 and 9 using 1 M
18
19
20 185 NaOH or HCl (Wei, Yu, et al., 2019). After stored for 24 h at 25 °C, the particle size and
21
22 186 zeta-potential were measured as described in section 2.3.

23
24
25 187 *2.5.5. Ionic stability*

26
27
28 188 Freshly prepared particle dispersions were mixed with different quantities of
29
30
31 189 NaCl powder for 2 h to ensure full interaction between the complex nanoparticles and
32
33
34 190 different ions. The NaCl concentration in different samples was adjusted to 10, 50, and
35
36 191 100 mM, respectively (Dai, Wei, et al., 2018a). After storage for 24 h, the particle size
37
38
39 192 and zeta-potential were measured as described in section 2.3.

40
41
42 193

43
44
45 194 *2.6. Storage stability*

46
47 195 Freshly prepared particle dispersions were incubated in temperature-controlled
48
49
50 196 chambers (4, 37 and 55 °C) for one week (Wei, Yang, et al., 2020). The particle size and
51
52
53 197 retention rate of curcumin in the complex nanoparticles were measured after 7 days as
54
55 198 described in section 2.3 and 2.4.

56
57
58 199

1 200 2.7. *Fluorescence spectroscopy*

2
3 201 Fluorescence of the particle dispersions was determined through a fluorescence
4
5
6 202 spectrophotometer (F-7000, Hitachi, Tokyo, Japan). The excitation wavelength was set
7
8
9 203 at 280 nm, and the emission spectra were collected between 290 and 450 nm with a
10
11
12 204 scanning speed of 100 nm/min (Sun, Wei, Li, Dai, & Gao, 2017a). Intrinsic
13
14
15 205 fluorescence of the protein was measured at a constant concentration of 0.2 mg/mL. All
16
17
18 206 data were collected at 25 °C, and each emission spectrum was the average of three runs.

19
20 207

21
22 208 2.8. *Circular dichroism (CD) spectroscopy*

23
24
25 209 The far-UV CD spectra (190-250 nm) were recorded using a CD
26
27
28 210 spectropolarimeter (Pistar π -180, Applied Photophysics Ltd., Surrey, UK) (Wei et al.,
29
30
31 211 2018). After a proper dilution of samples, the protein concentration was 0.2 mg/mL and
32
33
34 212 path length was 0.1 cm with constant nitrogen flush during data acquisition. Ellipticity
35
36
37 213 was recorded at a rate of 100 nm/min, 0.2 nm resolution, 20 accumulations, and 2.0 nm
38
39
40 214 bandwidth.

41
42 215

43
44
45 216 2.9. *Fourier transform infrared spectroscopy (FTIR)*

46
47 217 FTIR was applied to characterize the vibration of functional groups of zein, PGA,
48
49
50 218 curcumin and curcumin loaded binary complexes. Infrared spectra of freeze-dried
51
52
53 219 powders were recorded using a Spectrum 100 Fourier transform spectrophotometer
54
55
56 220 (PerkinElmer, Waltham, MA, USA). The spectra were acquired after 64 scans at a
57
58
59 221 wavenumber range from 4000 to 400 cm^{-1} with a 4 cm^{-1} resolution (Wei et al., 2018).

1 222

2
3 223 *2.10. X-ray diffraction (XRD)*

4
5
6 224 The molecular arrangement of samples was measured by an X-ray diffractometer
7
8
9 225 (Bruker D8, Odelzhausen, Germany) with a Cu anode, 40 kV voltage and current of
10
11 226 40 mA. The 2θ scan was fixed at 3° to 40° with a step size of 0.02° and step time of 5
12
13
14 227 s (Huang et al., 2017).

15
16
17 228

18
19
20 229 *2.11. Field emission scanning electron microscopy (FE-SEM)*

21
22 230 The morphology of samples was observed using a field emission scanning electron
23
24
25 231 microscopy (FE-SEM, SU8010, Hitachi, Tokyo, Japan). The samples were put on a
26
27
28 232 double-sided adhesive coated with a thin layer of gold and measured under 20.0 kV
29
30
31 233 acceleration voltage (Wei, Yu, et al., 2019).

32
33
34 234

35
36 235 *2.12. In vitro gastrointestinal digestion and bioaccessibility of curcumin*

37
38
39 236 All samples were digested with simulated gastric fluids (SGF) and simulated
40
41
42 237 intestinal fluids (SIF) according to the international digestion protocol (Minekus et al.,
43
44
45 238 2014). The pH value of SGF was adjusted to 2.0 using 1 M HCl and 30 mL of the
46
47
48 239 particle dispersion was incubated at 37°C for 1 h with 60 mL of SGF. The pH value of
49
50
51 240 gastric digesta and SIF was adjusted to pH 7.0 using 1 M NaOH. After the digestion in
52
53
54 241 stomach phase, 40 mL of gastric digesta was mixed with 40 mL of SIF and incubated
55
56 242 for 2 h at 37°C .

57
58 243 Determinations of particle size, curcumin **release percentage** and microstructure

1 244 were carried out after samples were exposed to each stage. The curcumin **release**
2
3 245 **percentage** was determined after each phase of digestion (Fan, Liu, Gao, Zhang, & Yi,
4
5
6 246 2018). An aliquot of raw digesta was centrifuged at 10000 rpm for 30 min at 10 °C, and
7
8
9 247 the supernatant was filtered with a 0.45 µm filter. Thereafter, the amount of curcumin
10
11
12 248 released from each sample was determined as described in section 2.4. The curcumin
13
14 249 **release percentage** (%) was calculated by following equation 3:

15
16
17 250
$$\text{Release percentage (\%)} = \frac{\text{released curcumin (mg)}}{\text{entrapped curcumin (mg)}} \times 100 \quad (3)$$

18
19

20 251 The bioaccessibility of curcumin was determined after the intestinal digestion. Part
21
22 252 of the digesta was processed using a high-speed centrifuge at 15,000 rpm for 60 min at
23
24
25 253 4 °C and the micelle phase containing the solubilized curcumin was collected. The
26
27
28 254 bioaccessibility of curcumin was defined as the fraction of curcumin released from the
29
30
31 255 food matrix and solubilized within mixed micelles present in the small intestine before
32
33
34 256 it could be absorbed (Yao, Xiao, & McClements, 2014). The curcumin contents
35
36
37 257 extracted from the initial nanoparticles and micelle fraction were determined according
38
39
40 258 to the method described in section 2.4. The bioaccessibility (%) of curcumin was
41
42
43 259 calculated by following equation 4:

44
45 260
$$\text{Bioaccessibility (\%)} = \frac{C_{micelle}}{C_{initial\ nanoparticle}} \times 100 \quad (4)$$

46

47 261 where $C_{micelle}$ represented the concentration of curcumin in the micelle fraction and
48
49
50 262 $C_{initial\ nanoparticle}$ represented the total concentration of curcumin encapsulated into the
51
52
53 263 **complex nanoparticles.**

54
55
56 264

57
58 265 *2.13. Statistical analysis*
59
60

1 266 All the data obtained were average values of triplicate determinations and
2
3 267 subjected to statistical analysis of variance using SPSS 18.0 for Windows (SPSS Inc.,
4
5
6 268 Chicago, USA). Statistical differences were determined by one-way analysis of
7
8
9 269 variance (ANOVA) with Duncan's post hoc test and least significant difference ($p < 0.05$)
10
11 270 was accepted among the treatments.

12
13
14 271

15 16 17 272 **3. Results and discussion**

18 19 20 273 *3.1. Particle size and zeta-potential*

21
22 274 The effects of HPM, heating and the combined treatments on the size and charge
23
24
25 275 properties of zein-PGA complex nanoparticles were evaluated. As shown in Fig. 1A,
26
27
28 276 the largest size (580.7 ± 12.2 nm) was observed in ZP without any external processing.
29
30
31 277 With the aid of HPM, the particle size was significantly ($p < 0.05$) reduced in ZP-50MPa
32
33
34 278 (320.6 ± 5.1 nm). With the rise in pressure level, the particle size was slightly decreased
35
36
37 279 and the smallest size was obtained in ZP-125MPa (299.3 ± 7.8 nm), which
38
39 280 demonstrated that HPM induced a reduction in the size of the complex nanoparticles.
40
41
42 281 As reported previously, the appropriate pressure might dissociate the aggregates of zein
43
44
45 282 molecules into smaller fragments, but higher pressure could result in the aggregation of
46
47
48 283 zein molecules (Sun, Yang, et al., 2016). A similar phenomenon was found in several
49
50
51 284 water soluble proteins, such as β -lactoglobulin (Zhong et al., 2014), soy protein (Song
52
53 285 et al., 2013) and peanut protein (Hu et al., 2011). **In our study, HPM showed a more**
54
55
56 286 **significant effect on the formation process of the complex nanoparticles through the**
57
58
59 287 **emulsification-evaporation method.** At the higher pressure, the protein molecules were

1 288 partially unfolded and exposed more active sites, which fully interacted with and bound
2
3 289 to the polysaccharide to form the compact and stable complexes. Therefore, compared
4
5
6 290 to zein nanoparticles, there was a more noticeable reduction in the size of zein-PGA
7
8
9 291 complex nanoparticles. However, irregular fluctuation occurred in the zeta-potential of
10
11
12 292 the complex nanoparticles as the pressure was elevated.

13
14 293 At the fixed homogenization pressure, the impact of different heating temperatures
15
16
17 294 on the size of zein-PGA complex nanoparticles was investigated (Fig. 1B). An obvious
18
19
20 295 increase in the particle size was observed after thermal processing. All the samples
21
22
23 296 exhibited a noticeable elevation in the particle size after heating at different
24
25
26 297 temperatures. After heating at 45 °C for 30 min, the size of zein-PGA complex
27
28
29 298 nanoparticles was increased from 318.4 ± 6.0 nm to 372.4 ± 14.9 nm. When the heating
30
31
32 299 temperature was elevated continuously, the size of zein-PGA complex nanoparticles
33
34
35 300 was increased slightly. Based on the previous studies, heating was generally used in
36
37
38 301 combinaton with other treatments to promote the alteration in protein structure and
39
40
41 302 improvement of functional properties, but the effect of thermal treatment alone was
42
43
44 303 very limited (Kim & Xu, 2008; Selling et al., 2007; Zhang et al., 2011). In the relevant
45
46
47 304 article, Sun et al. (2016) explored the influence of different heating temperatures on the
48
49
50 305 formation of zein colloidal particles. **The result showed that the increase in temperature**
51
52
53 306 **from 75 to 95 °C had no significant effect on the size and microstructure of zein**
54
55
56 307 **nanoparticles.** This phenomenon was consistent with the findings of this study:
57
58
59 308 **Although thermal treatment could promote the aggregation and structural**
60
61
62 309 **transformation of the complex nanoparticles, the increasing temperature showed a**

1 310 **limited impact on the complex nanoparticles.** Besides, according to our previous
2
3
4 311 research, the incorporation of PGA could effectively enhance the thermal stability of
5
6 312 zein and form more stable complex nanoparticles, thereby reducing the effect of
7
8
9 313 elevated temperature (Sun, Wei, Li, Dai, & Gao, 2017c; Wei et al., 2018).

10
11 314 Fig. 1C showed the influence of simultaneous HPM and thermal treatment on the
12
13
14 315 particle size and zeta-potential of the control group. After the combined treatment, the
15
16
17 316 size of most of nanoparticles was decreased significantly ($p<0.05$) except single zein
18
19
20 317 nanoparticles without curcumin. **As aforementioned, HPM induced a reduction in the**
21
22
23 318 **particle size, but thermal treatment conversely promoted the particle aggregation.** The
24
25
26 319 phenomenon demonstrated that HPM had a dominant impact on the size of zein-PGA
27
28
29 320 complex nanoparticles with the combination of HPM and heating. The external
30
31
32 321 processing exhibited a more significant impact on the size of zein-PGA complex
33
34
35 322 nanoparticles than that of individual zein, **revealing that the combined treatments**
36
37
38 323 **exerted a higher magnitude to modify the protein-polysaccharide complexes.** It was
39
40
41 324 noted that the zeta-potential of zein nanoparticles was significantly ($p<0.05$) decreased
42
43
44 325 after the encapsulation of curcumin, which was consistent with many previous studies
45
46
47 326 (Dai, Li, et al., 2018; Patel, Hu, Tiwari, & Velikov, 2010; Patel, Bouwens, & Velikov,
48
49
50 327 2010). Protein and curcumin mainly complexed through hydrogen bonds and
51
52
53 328 hydrophobic interaction to form a complex. Therefore, the encapsulation and
54
55
56 329 adsorption of curcumin may shield the surface charge of some amino acids, thereby
57
58
59 330 reducing the zeta-potential of the particles. Patel et al. (2010) reported that as the
60
61
62 331 content of curcumin increased, the zeta-potential of zein nanoparticles loaded with

1 332 curcumin continued to decrease. This result might indicate that the adsorption of excess
2
3 333 curcumin on the surface of the particles increase the attraction between the particles
4
5
6 334 and promote the aggregation of the particles.
7
8

9 335

10 336 *3.2. Encapsulation efficiency and loading capacity*

11 337 In order to assess the impact of different external treatments on the delivery of
12
13 338 curcumin with the complex nanoparticles, the encapsulation efficiency (EE) and
14
15
16 339 loading capacity (LC) of curcumin were determined. Among all the zein-PGA binary
17
18
19 340 complex nanoparticles, ZP exhibited the highest EE of 95.33% with the highest LC of
20
21
22 341 9.58% (Fig. 2A). After HPM treatment, the EE and LC were significantly ($p<0.05$)
23
24
25
26 342 decreased at 50 MPa, indicating that the extra homogenization process resulted in an
27
28
29 343 inevitable loss of curcumin. With the rise in HPM pressure, the EE of curcumin in zein-
30
31
32 344 PGA complex nanoparticles was continuously elevated and reached a maximum
33
34
35 345 (95.29%) at 100 MPa with the LC of 9.57%. The findings revealed that HPM treatment
36
37
38 346 with an appropriate pressure level facilitated the intermolecular interactions between
39
40
41 347 biopolymers and curcumin, which was also reported by other researchers (Chen, Wang,
42
43
44 348 Feng, Jiang, & Miao, 2019; Guo, Zhao, Chen, Chen, & Zheng, 2019). Nevertheless, the
45
46
47 349 EE and LC were slightly decreased after being processed over 100 MPa. The higher
48
49
50 350 pressure homogenization might cause a slight degradation of entrapped curcumin due
51
52
53 351 to the rise in processing temperature generated by extrusion and friction.

54 352 The influence of thermal treatment on the EE and LC was shown in Fig. 2B.

55
56
57 353 Compared to ZP-100MPa, the EE and LC of curcumin in zein-PGA complex
58
59
60
61
62
63
64
65

1 354 nanoparticles were reduced after thermal treatment. With the rise in temperature from
2
3 355 45 to 65 °C, the EE in zein-PGA complex nanoparticles was decreased from 89.72% to
4
5
6 356 85.09%. Similarly, the LC of curcumin in the nanoparticles was slightly reduced from
7
8
9 357 9.01% to 8.73%. It is reasonable to assume that thermal treatment accelerated the
10
11
12 358 oxidation and degradation of curcumin in the complex nanoparticles (Dai, Wei, et al.,
13
14 359 2018a). As the temperature was elevated to 75 °C, the EE of curcumin in zein-PGA
15
16
17 360 complex nanoparticles was elevated to 92.57%. The combined HPM and thermal
18
19
20 361 treatment induced the alteration of protein structure and then influenced the molecular
21
22
23 362 interactions between different compounds, which altered the conformation of zein and
24
25
26 363 strengthened the molecular interactions between biopolymers and curcumin (Sun, Dai,
27
28 364 He, et al., 2016). With the rise in heating temperature, the side groups of hydrophobic
29
30
31 365 aromatic amino acids were gradually exposed. During the exposure of hydrophobic
32
33
34 366 amino acids, the internal structure of the complex nanoparticles was altered (Sun, Dai,
35
36
37 367 Liu, et al., 2016). This result caused curcumin not only to be embedded inside the
38
39
40 368 nanoparticles, but also to be adsorbed on the surface of the nanoparticles through the
41
42
43 369 hydrophobic effects, thereby increasing its embedding rate. When the temperature was
44
45
46 370 further elevated, an obvious declination of EE was observed in ZP-85°C,100MPa
47
48 371 (88.41%). Therefore, the pressure of 100 MPa and temperature at 75 °C were confirmed
49
50
51 372 to be the optimum parameters in the fabrication of curcumin loaded zein-PGA complex
52
53
54 373 nanoparticles. These results proved that the coupled microfluidization and thermal
55
56
57 374 treatment would have the potential to improve the EE and LC of protein-polysaccharide
58
59 375 complex nanoparticles for delivery of nutraceuticals.

1 376

2
3 377 *3.3. Physical stability*

4
5 378 The physical stability of different nanoparticles was analyzed through imposing
6
7 379 the centrifugal force. The fluctuation amplitude of the curves reflected the physical
8
9
10 380 stability of the nanoparticles. As shown in Fig. 3A, ZP-50MPa exhibited the best
11
12
13 381 physical stability among all the zein-PGA complex nanoparticles through HPM at
14
15
16 382 different pressures. The physical stability of the complex nanoparticles was gradually
17
18 383 reduced with HPM pressure rising. There was no obvious fluctuation in the size and
19
20
21 384 zeta-potential of zein-PGA complex nanoparticles (Fig. 1). Therefore, the good stability
22
23
24 385 of ZP-50MPa was mainly due to its lower content of curcumin (Fig. 2A). The
25
26
27 386 encapsulation of a small quantity of curcumin could promote the molecular interactions
28
29
30 387 between components (hydrophobic attraction and hydrogen bonding) to form a denser
31
32
33 388 structure. Nevertheless, at the higher content of curcumin, excessive curcumin could
34
35
36 389 adsorb on the particle surface and cause the particles to aggregate (A. Patel et al., 2010).

37
38 390 Thermal treatment showed an obvious effect on the physical stability of the
39
40
41 391 complex nanoparticles (Fig. 3B). At lower temperatures, ZP-55°C,100MPa exhibited
42
43
44 392 the best physical stability due to the smaller size and lower content of curcumin
45
46
47 393 encapsulated. According to Brownian motion and Stokes' law, the smaller size
48
49
50 394 diminished the sedimentation frequency of the nanoparticles and made them more
51
52
53 395 stable (Joye et al., 2015). Additionally, the lower content of encapsulated curcumin
54
55
56 396 enhanced the physical stability of the nanoparticles and contributed to the formation of
57
58
59 397 compact structure with reduced interparticle hydrophobic attraction (Fig. 2B) (Dai, Li,

1 398 et al., 2018; A. R. Patel et al., 2010; Wei et al., 2018).

2
3 399 Fig. 3C exhibits the physical stability of different control groups. Among all the
4
5
6 400 samples, Z and Z-cur were the most unstable due to their large size and strong
7
8
9 401 hydrophobicity. With the external HPM and thermal treatment, the physical stability of
10
11
12 402 Z-75°C, 100MPa and Z-cur-75°C, 100MPa was greatly improved. After the
13
14
15 403 complexation of zein with PGA, the stability of zein-PGA complex nanoparticles
16
17
18 404 became much better than that of zein nanoparticles due to the appropriate
19
20
21 405 amphiphilicity and enhanced repulsion (Wei et al., 2018). Moreover, ZP-75°C, 100MPa
22
23
24 406 exhibited a much better physical stability, which suggested that both HPM and thermal
25
26
27 407 treatment indeed improved the physical stability of zein-PGA complexes through
28
29
30 408 reducing the particle size (Fig. 1C), which was advantageous to expand their potential
31
32
33 409 applications in the commercial products.

34 410

35
36 411 *3.4. Physicochemical stability of curcumin loaded zein-PGA complex nanoparticles*
37
38
39 412 *under environmental stresses*

40
41
42 413 *3.4.1. Photo stability*

43
44 414 The photo stability of curcumin loaded in zein-PGA complex nanoparticles against
45
46
47 415 UV radiation was comprehensively evaluated. Among all the samples, the curcumin
48
49
50 416 encapsulated in ZP without external treatments exhibited the best chemical stability,
51
52
53 417 which remained more than 50% after the exposure to UV light for 2 h (Fig. 4A).
54
55
56 418 Nevertheless, the photo stability of curcumin in complex nanoparticles gradually
57
58
59 419 decreased with increasing homogenization pressure. The result interpreted that the

1 420 external homogenization might alter the microstructure of the complex nanoparticles
2
3 421 and molecular interactions between the components, thereby diminishing the chemical
4
5
6 422 stability of curcumin against UV radiation.
7

8
9 423 On the contrary, thermal treatment had the opposite influence on the photo stability
10
11 424 of curcumin entrapped in zein-PGA complex nanoparticles compared to HPM (Fig. 4B).
12
13
14 425 The photo stability of curcumin in ZP-45°C, 100MPa was slightly reduced compared to
15
16
17 426 that in ZP-100MPa. With the heating temperature rising, the photo stability of curcumin
18
19
20 427 in zein-PGA complex nanoparticles was slightly elevated along with thermal treatment.
21
22
23 428 The highest retention rate of curcumin was achieved in ZP-75°C, 100MPa after 120 min
24
25
26 429 of exposure to UV light. It was noted that thermal treatment at higher temperatures
27
28
29 430 could provide the complex nanoparticles with a better physical stability, which was
30
31
32 431 consistent with the improved chemical stability of curcumin. **It was assumed that**
33
34 432 **thermal treatment influenced the microstructure of the complex nanoparticles and**
35
36 433 **molecular interactions, which provided a better protection for curcumin (Dissanayake**
37
38
39 434 **& Vasiljevic, 2009).**

40 41 42 435 *3.4.2. Thermal stability*

43
44 436 The curcumin encapsulated in zein-PGA complex nanoparticles exhibited good
45
46
47 437 stability after heating at 85 °C for 30 min with the retention rate of curcumin over 90%
48
49
50 438 (Fig. 4C). Although individual thermal treatment and HPM improved thermal stability
51
52
53 439 of curcumin in the complex nanoparticles, a significant decrease in the retention rate of
54
55
56 440 curcumin was observed in ZP-75°C, 100MPa, showing a lack of synergistic effect
57
58
59 441 between HPM and thermal treatment on enhancing the thermal stability of curcumin

1 442 loaded in zein-PGA complex nanoparticles.
2

3 443 The influence of thermal processing on the size (Fig. 5A) and zeta-potential (Fig.
4
5
6 444 5B) of the complex nanoparticles was investigated. A slight increase was observed in
7
8
9 445 the size of zein-PGA complex nanoparticles without any external treatment, verifying
10
11
12 446 that the aggregation and sedimentation occurred due to thermal processing. It was
13
14
15 447 observed that HPM and thermal treatment could effectively enhance the physical
16
17 448 stability of zein-PGA complex nanoparticles. Besides, an obvious increase appeared in
18
19
20 449 the zeta-potential of all the complex nanoparticles, manifesting that the thermal
21
22
23 450 processing influenced the microstructure of the nanoparticles and altered their surface
24
25
26 451 properties. The enhanced thermal stability of the complex nanoparticles unraveled that
27
28
29 452 HPM and heating strengthened the resistance of the nanoparticles against thermal
30
31 453 treatment during industrial applications.

32 33 34 454 *3.4.3. pH stability* 35

36 455 The colloidal delivery systems would experience the pH fluctuation for their
37
38
39 456 applications in food products. As shown in Fig. 5C and D, the size and zeta-potential
40
41
42 457 of different complex nanoparticles were measured in distinct pH values. Compared to
43
44
45 458 the original state (pH 4), there was a slight increase in the size of zein-PGA complex
46
47
48 459 nanoparticles at pH 2. The particle size of ZP was increased from 648.3 ± 49.8 to
49
50
51 460 707.6 ± 54.7 nm as pH was decreased from 4 to 2, which was mainly attributed to the
52
53
54 461 reduced electrostatic repulsion between the nanoparticles with a reduced absolute zeta-
55
56
57 462 potential value (Wei, Yang, et al., 2020). With the coupled treatments of HPM and
58
59 463 heating, zein-PGA complex nanoparticles remained stable under acidic condition.
60

1 464 When the pH was moved to 6 and 9, the size of zein-PGA complex nanoparticles was
2
3 465 decreased significantly ($p<0.05$) with the rise in zeta-potential. For instance, the size of
4
5
6 466 ZP was decreased to 450.2 ± 39.8 and 372.7 ± 21.7 nm at pH 6 and 9, respectively. The
7
8
9 467 enhanced electrostatic repulsion kept the nanoparticles apart and prevented the
10
11
12 468 aggregation of the nanoparticles. Compared with ZP, the associated heating and
13
14
15 469 microfluidization processed complex nanoparticles kept more stable in response to pH
16
17
18 470 fluctuation. As the pH was elevated from 4 to 6 and 9, the size of ZP-75°C, 100MPa
19
20 471 was decreased from 432.8 ± 9.6 to 388.4 ± 11.8 and 326.2 ± 3.6 nm.

22 472 *3.4.4. Ionic strength stability*

25 473 The physical stability of different complex nanoparticles was investigated under
26
27
28 474 various ionic strengths (10, 50 and 100 mM). **The largest increase was observed in the**
29
30
31 475 **size of ZP with the ionic strength rising (Fig. 5E).** With the external HPM and thermal
32
33
34 476 treatment, the physical stability of zein-PGA complex nanoparticles was visibly
35
36
37 477 improved under various ionic strengths. Meanwhile, the absolute zeta-potential value
38
39
40 478 of the complex nanoparticles was gradually reduced as the ionic strength was increased
41
42
43 479 through electrostatic screening (Fig. 5F). Although the electrostatic repulsion was
44
45
46 480 limited, the size of zein-PGA complex nanoparticles still kept relatively stable with
47
48
49 481 HPM and thermal treatment, indicating that the external processing could enhance
50
51
52 482 physical stability of the nanoparticles at distinct ionic strengths.

53 483

56 484 *3.5. Storage stability*

58 485 To ascertain the storage stability of curcumin loaded zein-PGA complex

1 486 nanoparticles, different samples were stored for one week at 4, 37, and 55 °C. After
2
3 487 storage, the size of zein-PGA complex nanoparticles was increased to different
4
5
6 488 magnitudes (Fig. 6A). Interestingly, the largest increase in the particle size was
7
8
9 489 observed in the complex nanoparticles stored at 4 °C, which was larger than those stored
10
11 490 at 37 °C and 55 °C. Besides, it was noticed that the absolute zeta-potential value of the
12
13
14 491 nanoparticles was increased with the storage temperature rising, thereby providing the
15
16
17 492 sufficient electrostatic repulsion to keep the nanoparticles apart during storage period
18
19
20 493 (Fig. 6B), which might be attributed to the thermal degradation of curcumin (Dai, Wei,
21
22
23 494 et al., 2018b).

24
25 495 Fig. 6C shows the retention rate of curcumin encapsulated in zein-PGA complex
26
27
28 496 nanoparticles stored at different temperatures. It was clearly noted that the retention rate
29
30
31 497 of curcumin in the nanoparticles decreased with the storage temperature rising,
32
33
34 498 revealing that the higher temperature accelerated the chemical degradation of curcumin.
35
36
37 499 In terms of the storage stability of different nanoparticles, all the samples exhibited the
38
39
40 500 excellent protection of curcumin at 4 °C without significant differences. As the
41
42
43 501 temperature was elevated to 37 °C, ZP-75°C showed the best chemical stability of
44
45
46 502 curcumin among zein-PGA complex nanoparticles. When the nanoparticles were stored
47
48
49 503 at 55 °C, no obvious difference was found in zein-PGA complex nanoparticles.
50
51
52 504 Nevertheless, the coupled treatment of HPM and heating provided a better protection
53
54
55 505 for curcumin in the complex nanoparticles compared to individual HPM or thermal
56
57
58 506 treatment. As discussed above, the size and zeta-potential of the complex nanoparticles
59
60
61 507 seemed to be correlated with the thermal degradation of curcumin. The thermal
62
63
64
65

1 508 degradation of curcumin promoted the increase in absolute zeta-potential value and the
2
3 509 decrease in particle size (Fig. 6A and B), which was mainly ascribed to alteration of the
4
5
6 510 particle structure and molecular interactions. The degradation of curcumin caused by
7
8
9 511 the temperature rise weakened the hydrophobic interaction between the particles and
10
11 512 reduced the interparticle attraction. On the other hand, the rise in zeta-potential
12
13 513 increased the electrostatic repulsion between the particles, causing the particles to
14
15
16
17 514 separate from each other. These results testified that the combined HPM and thermal
18
19
20 515 treatment could extend the shelf-life of nanoparticle-based delivery vehicles.
21

22 516

23 517 *3.6. Fluorescence property*

24
25
26
27
28 518 Fluorescence is utilized to investigate the alteration in the polarity of surrounding
29
30 519 environment of fluorophore (Wei, Yu, et al., 2019), which can be utilized to assess the
31
32
33 520 molecular interactions between biopolymers and curcumin. As shown in Fig. 7, zein
34
35
36 521 exhibited a fluorescence emission peak at 304 nm after being excited at 280 nm, which
37
38
39 522 was attributed to its high proportion of tyrosine residues (Sun et al., 2017c; Wei et al.,
40
41
42 523 2018). Upon the encapsulation of curcumin, the tyrosine fluorescence got almost
43
44
45 524 quenched and the fluorescence intensity of Z-cur was greatly reduced, which was
46
47
48 525 consistent with the complexation of other proteins and polyphenols (Dai, Wei, et al.,
49
50 526 2018a; Joye et al., 2015; Liang, Tajmir-Riahi, & Subirade, 2008). Nevertheless, the
51
52
53 527 complexation of zein with PGA increased the fluorescence intensity of zein, indicating
54
55
56 528 a more apolar micro-environment of tyrosine residues (Wei et al., 2018). After HPM at
57
58
59 529 different pressures, the fluorescence intensity of the protein was decreased greatly,
60

1 530 which was consistent with the reports from other researchers (Fig. 7A) (Chen et al.,
2
3 531 2019; Sun, Yang, et al., 2016). The decreased fluorescence intensity might be ascribed
4
5
6 532 to the entanglement and aggregation of molecular chains generated by shear, impact
7
8
9 533 and vibration at a specific pressure (Dissanayake & Vasiljevic, 2009; O'Sullivan,
10
11 534 Arellano, Pichot, & Norton, 2014). In zein-PGA complex nanoparticles, most of
12
13
14 535 aromatic amino acids that could produce fluorescence were inside the zein molecule,
15
16
17 536 and the locally environmental polarity was less than that of the aqueous solution for the
18
19
20 537 nanoparticles. During the denaturation of zein, the side chain groups of aromatic amino
21
22
23 538 acid molecules were gradually exposed, and the increased environmental polarity of
24
25
26 539 amino acid molecules resulted in a decrease in fluorescence intensity (Liang et al.,
27
28 540 2008).

30
31 541 The thermal treatment also decreased the fluorescence intensity of zein slightly
32
33
34 542 with the rise in the heating temperature (Fig. 7B). During thermal processing, the
35
36
37 543 conformation of zein underwent some changes, which exposed the amino acid residues
38
39
40 544 buried inside the native structure, leading to a decrease in the fluorescence intensity
41
42
43 545 (Sun, Dai, He, et al., 2016). However, in control groups, the external processing of HPM
44
45
46 546 and heat exhibited much less influence on zein-PGA complex nanoparticles in the
47
48
49 547 absence of curcumin (Fig. 7C). The fluorescence intensity of zein in Z-P was decreased
50
51
52 548 slightly during the coupled treatment of HPM and heating. The phenomenon testified
53
54
55 549 that the structure of the complex nanoparticles was very stable without curcumin. The
56
57
58 550 incorporation of PGA indeed provided an effective protection for the conformation of
59
60
61 551 zein during external processing (Sun, Dai, He, et al., 2016; Sun, Yang, et al., 2016).

1 552

2
3 553 *3.7. Circular dichroism*

4
5
6 554 The alterations in CD signals are easily assigned to distinct structural features of
7
8
9 555 proteins. The different types of regular secondary structure found in proteins give rise
10
11 556 to characteristic CD spectra in the far UV (Kelly, Jess, & Price, 2005). The secondary
12
13 557 structure of zein was calculated by CD in the far-UV range (260–190 nm) by SELCON
14
15
16
17 558 3 on an online server DICHROWEB (Fig. 8). The secondary structure of zein contained
18
19
20 559 more than 50% α -helix (Wei et al., 2018). It was noted that the process of
21
22 560 emulsification-evaporation decreased the content of α -helix and then increased the
23
24
25 561 content of β -sheet accordingly (Selling et al., 2007), revealing the disorder-to-order
26
27
28 562 state of secondary structure (Dyson & Wright, 2005).

29
30
31 563 The α -helix content of zein was greatly increased from 11.9% (zein colloidal
32
33 564 particles) to 43.7% (ZP), indicating that the α -helix structure in zein-PGA complex
34
35
36 565 nanoparticles was effectively protected (Fig. 8A). Nevertheless, HPM treatment at the
37
38
39 566 pressure of 50 MPa led to a dramatic decrease of α -helix fraction from 44.3% to 16.0%
40
41
42 567 and an increase of β -sheet fraction from 13.1% to 32.5% in zein-PGA complex
43
44
45 568 nanoparticles. The results revealed that HPM induced the unfolding and aggregation of
46
47
48 569 proteins, and promoted the transition from α -helix to β -sheet in the secondary structure
49
50
51 570 of zein. The HPM-induced intermolecular β -sheet aggregation enhanced the
52
53 571 microstructural stability of the nanoparticles, which was consistent with the decreased
54
55
56 572 fluorescence intensity (Sun, Wei, Li, Dai, & Gao, 2017b; Wei, Yu, et al., 2019). With
57
58
59 573 the increase in the pressure from 50 to 150 MPa, there was a slight increase in α -helix

1 574 fraction of zein-PGA complex nanoparticles (Fig. 8B), manifesting that structural
2
3 575 rearrangement of zein molecules was generated by microfluidization at the higher
4
5
6 576 pressure (Sun, Dai, Liu, et al., 2016).
7

8
9 577 Thermal treatment of zein-PGA complex nanoparticles resulted in a slight increase
10
11 578 in α -helix fraction and a decrease in β -sheet fraction (Fig. 8C), which verified the
12
13 579 hypothesis that zein molecular chains were partially unfolded due to thermal treatment.
14
15
16 580 Compared with single HPM, the coupled treatment of HPM and heating showed
17
18
19 581 different impacts on modulating the secondary structure of zein, especially at 55 °C. The
20
21
22 582 results clearly revealed that HPM had a more significant effect on the conformational
23
24
25 583 change of zein compared to thermal treatment, which was consistent with the
26
27
28 584 fluorescence intensity of zein.
29
30

31 585

32 33 586 3.8. FTIR

34
35
36 587 FTIR technique is a versatile tool to monitor change in the functional groups of
37
38
39 588 biopolymers and analyze the intermolecular interactions between zein, PGA and
40
41
42 589 curcumin during the formation of the complex nanoparticles (Fig. 9A). Two major
43
44
45 590 characteristic peaks of zein were observed at around 1658.1 and 1540.7 cm^{-1} , which
46
47
48 591 were indicatives of the amide I band (1750-1600 cm^{-1}) and amide II band (1550-1510
49
50
51 592 cm^{-1}). An absorption band of O-H stretching was found at 3311.2 cm^{-1} . The curcumin
52
53
54 593 spectrum showed characteristics peaks at 1602.0, 1583.1, 1512.1, 1455.7, 1375.2, and
55
56
57 594 963.4 cm^{-1} , probably due to aromatic -C=C- stretching, olefinic -C-C- stretching,
58
59
60 595 aromatic ring C=C- stretching, aromatic ring -C=C- stretching, -C-O- stretching
61
62
63
64
65

1 596 vibration, and trans olefinic -C=C- stretching, respectively (Dai, Wei, et al., 2018b; Fan
2
3 597 et al., 2018). After the complexation of zein with PGA, the intensity of absorption peak
4
5
6 598 corresponding to hydrogen bonds and amide II band was obviously increased. This was
7
8
9 599 attributed to the intermolecular hydrogen bonding and electrostatic interaction, which
10
11
12 600 mainly contributed to the formation of zein-PGA complex nanoparticles.

13
14 601 The influence of HPM pressure on the structure and molecular interactions of zein-
15
16
17 602 PGA complex nanoparticles was demonstrated in Fig. 9B. With the homogenizing
18
19
20 603 pressure increasing, the intensity of absorbance peaks at around 1660 and 3310 cm^{-1}
21
22
23 604 was continuously elevated due to the formation of β -sheet aggregates through
24
25
26 605 intermolecular hydrogen bonding. The conformational change of the protein has been
27
28
29 606 confirmed by the fluorescence intensity and circular dichroism. During thermal
30
31
32 607 treatment, the intensity of absorption peaks corresponding to amide band I and
33
34
35 608 hydrogen bonding was slightly decreased with the rise in heating temperature, which
36
37
38 609 meant that thermal treatment promoted the transition from β -sheet into α -helix and
39
40
41 610 interrupted the intermolecular hydrogen bonding (Fig. 9C). Besides, the reduction of β -
42
43
44 611 sheet regions at the interface of proteins was related to the conformational freedom in
45
46
47 612 the protein structure and aggregation of the particles (Lefèvre, Subirade, & Pérolet,
48
49
50 613 2005; Mangavel, Barbot, Popineau, & Guéguen, 2001).

51 614

52 615 3.9. X-ray diffraction

53
54
55 616 Fig. 10 showed the crystalline diffraction patterns of pure curcumin, zein, PGA,
56
57
58 617 and zein-PGA complex particles. For individual biopolymers, zein and PGA had

1 618 relatively flat peaks, which interpreted the amorphous nature of biopolymers (Fig. 10A).
2
3 619 On the contrary, pure curcumin was highly crystallized with characteristic sharp
4
5
6 620 diffraction peaks. Nevertheless, there were no obvious diffraction peaks belonging to
7
8
9 621 curcumin after its encapsulation into zein-PGA binary complex nanoparticles with an
10
11 622 amorphous state. Compared to individual zein and PGA, the diffraction peaks of zein-
12
13 623 PGA complex nanoparticles at previous angles further decreased and even disappeared,
14
15
16
17 624 interpreting that the intermolecular interactions among individual components altered
18
19
20 625 the physical state in the formation of the complex nanoparticles (Sun et al., 2017b).
21

22
23 626 The different homogenization pressures could scarcely exhibit the obvious
24
25 627 influence on the XRD spectra of zein-PGA complex nanoparticles in an amorphous
26
27
28 628 state (Fig. 10B). The thermal treatment showed different effects on the molecular
29
30
31 629 structure of the complex nanoparticles. Among zein-PGA complex nanoparticles, the
32
33 630 diffraction intensity of the nanoparticles was increased firstly and then decreased with
34
35
36 631 the heating temperature rising (Fig. 10B). The findings were attributed to distinct
37
38
39 632 microstructures of the complex nanoparticles induced by different heating temperatures
40
41
42 633 (Dai, Wei, et al., 2018b; Wei, Zhang, et al., 2019). As evidenced by circular dichroism,
43
44 634 in the secondary structure of zein, the proportion of α -helix was reduced and the fraction
45
46
47 635 of β -helix was increased progressively when the temperature was elevated from 65 to
48
49
50 636 85 °C.
51

52
53 637

54 55 638 *3.10. Morphology*

56
57
58 639 The morphological features of the complex nanoparticles were observed with the
59

1 640 aid of FE-SEM. As shown in Fig. 11, ZP without curcumin entrapped exhibited a
2
3 641 regular shape with the rough surface, which was difficult to distinguish individual
4
5
6 642 nanoparticles. The connection among the nanoparticles was provided by excessive PGA
7
8
9 643 adsorbed on the surface of complex nanoparticles as interparticle bridges (Wei et al.,
10
11 644 2018). After the coupled treatments of HPM and heating, the long molecular chains of
12
13
14 645 PGA could fold and interact fully with zein molecules, thereby forming spherical
15
16
17 646 complex nanoparticles. Interestingly, after the encapsulation of curcumin, ZP exhibited
18
19
20 647 a more uniform size distribution, which might be because the curcumin entrapped
21
22
23 648 enhanced the hydrophobic effect inside the nanoparticles, thus forming a denser
24
25
26 649 structure. With the combined HPM and heating, the size of ZP-75°C,100MPa was
27
28
29 650 visibly reduced, but partial aggregation of the nanoparticles occurred (Sun, Dai, Liu, et
30
31 651 al., 2016). The phenomenon was reasonably attributable to the enhanced hydrophobic
32
33
34 652 attraction between the nanoparticles due to the external treatment.
35

36 653

39 654 3.11. *In vitro* gastrointestinal digestion

42 655 The digestion behavior of curcumin loaded complex nanoparticles was
43
44 656 investigated in the simulated GI tract. The size of the nanoparticles during *in vitro*
45
46
47 657 digestion was dependent on the digestion time in the simulated GI tract. As shown in
48
49
50 658 Fig. 12A, the particle size kept stable or even decreased slightly after exposure to the
51
52
53 659 gastric phase. The phenomenon was consistent with our previous study, which reported
54
55
56 660 the digestion fate of β -carotene loaded zein-PGA nanoparticles (Wei et al., 2018). The
57
58
59 661 result implied that zein-PGA complex nanoparticles exhibited a better stability in the

1 662 stomach phase against pepsin. There was a stepwise increase in the size of curcumin
2
3 663 loaded complex nanoparticles after exposure to the small intestine phase, revealing that
4
5
6 664 the structure of the complex nanoparticles was gradually broken down in the small
7
8
9 665 intestine.

10
11 666 The **release percentages** of curcumin in the complex nanoparticles at 30, 60, 90,
12
13
14 667 120, 150- and 180-min during GIT are shown in Fig. 12B. The lowest **release**
15
16
17 668 **percentage** ($11.43 \pm 0.97\%$) of curcumin in the gastric phase was obtained in zein-PGA
18
19
20 669 complex nanoparticles without any external processing. After HPM processing at
21
22
23 670 different pressures, the shear, impact and vibration within microfluidization caused the
24
25
26 671 entanglement and aggregation of molecular chains in zein. In zein-PGA complex
27
28
29 672 nanoparticles, the side chain groups of aromatic amino acid molecules were gradually
30
31
32 673 exposed, the internal structure of the complex nanoparticles was altered, and the
33
34
35 674 hydrophobic interaction between curcumin and zein was destroyed, promoting the
36
37
38 675 release of curcumin from the nanoparticles in the gastric phase. After thermal treatment,
39
40
41 676 the conformation of zein underwent an obvious alteration, which also exposed the
42
43
44 677 amino acid residues buried inside the native structure, thus slightly facilitating the
45
46
47 678 release of curcumin from zein-PGA complex nanoparticles.

48 679 After being digested for 180 min, most of curcumin in the complex nanoparticles
49
50
51 680 was released in the intestine, especially at initial 30 min. Among zein-PGA complex
52
53
54 681 nanoparticles, ZP-75°C showed the highest **release percentage** of curcumin ($98.95 \pm$
55
56
57 682 0.24%) in the intestine phase. Additionally, ZP-75°C, 100MPa exhibited the lowest
58
59
60 683 **release percentage** ($81.93 \pm 0.74\%$) after the coupled treatments of HPM and heating.

1 684 The results revealed that zein-PGA complex nanoparticles without any external
2
3 685 processing showed the highest release percentage of curcumin due to their looser
4
5
6 686 structure, thereby accelerating the release of curcumin in the gastric phase.
7

8
9 687 Different from the release percentage of curcumin, ZP exhibited the lowest
10
11 688 bioaccessibility ($12.31 \pm 0.64\%$) (Fig. 12C). With individual HPM or thermal treatment,
12
13
14 689 the bioaccessibility of curcumin was slightly improved compared to ZP. After the
15
16
17 690 coupled treatments of HPM and heating, the curcumin bioaccessibility was
18
19
20 691 significantly ($p < 0.05$) elevated to a higher level ($52.35 \pm 1.58\%$) in ZP-75°C,100MPa.
21
22 692 Although individual HPM or thermal treatment could enhance the bioaccessibility of
23
24
25 693 curcumin during *in vitro* digestion, the HPM and thermal treatment exhibited a greater
26
27
28 694 effect on enhancing the bioaccessibility of curcumin, and even its bioaccessibility was
29
30
31 695 higher than the sum of bioaccessibility of curcumin loaded in the nanoparticles with
32
33
34 696 two individual treatments. Therefore, HPM and heat treatment showed not only a
35
36
37 697 simple additive effect, but a synergistic effect on enhancing the bioaccessibility of
38
39
40 698 curcumin. The more uniform size and compact structure promoted to elevate
41
42
43 699 significantly ($p < 0.05$) the bioaccessibility of curcumin in the small intestine phase
44
45
46 700 from zein-PGA complex nanoparticles, which might increase the adsorption of bile salts
47
48
49 701 and digestive enzyme onto the nanoparticle surface. The strengthened interactions
50
51
52 702 between the complex nanoparticles and SIF enhanced the release of curcumin and
53
54
55 703 formation of mixed micelles (Fan et al., 2018).
56

57
58 704 The FE-SEM images revealed that the morphology of the complex nanoparticles
59
60 705 almost kept stable after simulated gastric digestion (Fig. 12D), which was dominantly
61
62
63
64
65

1 706 ascribed to the resistance of zein against pepsin in the gastric phase (A. R. Patel &
2
3 707 Velikov, 2014; Penalva et al., 2015; Wei et al., 2018). After exposure to the small
4
5
6 708 intestine phase for 120 min, zein-PGA complex nanoparticles were collapsed in shape
7
8
9 709 and agglomerated. The digestion of zein by pancreatin led to a distorted shape and more
10
11
12 710 release of curcumin. The aggregation of zein-PGA complex nanoparticles obviously
13
14
15 711 occurred in the intestinal phase, thereby limiting the **release percentage** and
16
17
18 712 bioaccessibility of curcumin in the nanoparticles during the intestinal digestion.
19
20
21 713

22

23 714 **4. Conclusion**

24
25
26 715 In the present study, the microfluidization pressure at 100 MPa and heating
27
28
29 716 temperature at 75 °C were the optimum parameters for providing a better protection of
30
31
32 717 curcumin entrapped in zein-PGA complex nanoparticles. With the treatment of HPM,
33
34
35 718 the complex nanoparticles exhibited a better stability under various environmental
36
37
38 719 stresses (pH, ionic strength, light and heat) and storage conditions (37 and 55 °C).
39
40
41 720 Nevertheless, compared with single HPM treatment, the combined HPM and thermal
42
43
44 721 treatment did not show a significant advantage in improving the stability and functional
45
46
47 722 properties of the complex nanoparticles. Through the observation of FE-SEM, HPM
48
49
50 723 and thermal treatment facilitated the formation of zein-PGA complex nanoparticles
51
52
53 724 with a more uniform size and spherical shape. *In vitro* digestion model revealed that
54
55
56 725 the complex nanoparticles exhibited the excellent gastric stability and sustained-release
57
58
59 726 of curcumin in the small intestine phase. Notably, the bioaccessibility of curcumin
60
61
62 727 was enhanced after the coupled treatment of HPM and heating. The findings from this

1 728 study confirmed that HPM alone could effectively enhance the functional attributes,
2
3 729 environmental stability, and sustained-release of curcumin-loaded protein-
4
5
6 730 polysaccharide complex nanoparticles. A new insight into the potential application of
7
8
9 731 HPM and heating is provided in the design and development of nanoparticle-based
10
11
12 732 delivery vehicles.

14 **Corresponding Author**

15
16
17
18 *E-mail: gyxcau@126.com
19
20

21 **Notes**

22
23
24 The authors declare no competing financial interest.
25
26

27 **Acknowledgement**

28
29
30 Financial support from the National Natural Science Foundation of China
31
32 (No.31871842) is gratefully acknowledged. We acknowledge Jianhui Li from the
33
34 Institute of Biophysics, China Academy of Sciences, for performing the circular
35
36 dichroism analysis.
37
38
39
40

41 **References:**

- 42
43
44 733 Chen, G., Wang, S., Feng, B., Jiang, B., & Miao, M. (2019). Interaction between
45
46 734 soybean protein and tea polyphenols under high pressure. *Food Chemistry*,
47
48
49 735 277(November 2018), 632–638. <https://doi.org/10.1016/j.foodchem.2018.11.024>
50
51
52 736 Dai, L., Li, R., Wei, Y., Sun, C., Mao, L., & Gao, Y. (2018). Fabrication of zein and
53
54
55 737 rhamnolipid complex nanoparticles to enhance the stability and in vitro release of
56
57
58 738 curcumin. *Food Hydrocolloids*, 77, 617–628.
59
60

- 1 739 <https://doi.org/10.1016/j.foodhyd.2017.11.003>
2
3
4 740 Dai, L., Sun, C., Li, R., Mao, L., Liu, F., & Gao, Y. (2017). Structural characterization,
5
6 741 formation mechanism and stability of curcumin in zein-lecithin composite
7
8
9 742 nanoparticles fabricated by antisolvent co-precipitation. *Food Chemistry*, 237,
10
11 743 1163–1171. <https://doi.org/10.1016/j.foodchem.2017.05.134>
12
13
14 744 Dai, L., Wei, Y., Sun, C., Mao, L., McClements, D. J., & Gao, Y. (2018a). Development
15
16 745 of protein-polysaccharide-surfactant ternary complex particles as delivery
17
18 746 vehicles for curcumin. *Food Hydrocolloids*, 85(17), 75–85.
19
20
21 747 <https://doi.org/10.1016/j.foodhyd.2018.06.052>
22
23
24
25 748 Dai, L., Wei, Y., Sun, C., Mao, L., McClements, D. J., & Gao, Y. (2018b).
26
27 749 Development of protein-polysaccharide-surfactant ternary complex particles as
28
29 750 delivery vehicles for curcumin. *Food Hydrocolloids*, 85(17), 75–85.
30
31
32 751 <https://doi.org/10.1016/j.foodhyd.2018.06.052>
33
34
35
36 752 Dissanayake, M., & Vasiljevic, T. (2009). Functional properties of whey proteins
37
38 753 affected by heat treatment and hydrodynamic high-pressure shearing. *Journal of*
39
40 754 *Dairy Science*, 92(4), 1387–1397. <https://doi.org/10.3168/jds.2008-1791>
41
42
43
44 755 Dyson, H. J., & Wright, P. E. (2005). Intrinsically unstructured proteins and their
45
46 756 functions. *Nature Reviews Molecular Cell Biology*, 6(3), 197–208.
47
48
49 757 <https://doi.org/10.1038/nrm1589>
50
51
52
53 758 Fan, Y., Liu, Y., Gao, L., Zhang, Y., & Yi, J. (2018). Improved chemical stability and
54
55 759 cellular antioxidant activity of resveratrol in zein nanoparticle with bovine serum
56
57 760 albumin-caffeic acid conjugate. *Food Chemistry*, 261, 283–291.
58
59
60

1 761 <https://doi.org/10.1016/J.FOODCHEM.2018.04.055>
2
3 762 Guo, Z., Zhao, B., Chen, J., Chen, L., & Zheng, B. (2019). Insight into the
4
5
6 763 characterization and digestion of lotus seed starch-tea polyphenol complexes
7
8
9 764 prepared under high hydrostatic pressure. *Food Chemistry*, 297(March).
10
11 765 <https://doi.org/10.1016/j.foodchem.2019.124992>
12
13 766 Hu, X., Zhao, M., Sun, W., Zhao, G., & Ren, J. (2011). Effects of microfluidization
14
15
16 767 treatment and transglutaminase cross-linking on physicochemical, functional, and
17
18
19 768 conformational properties of peanut protein isolate. *Journal of Agricultural and*
20
21
22 769 *Food Chemistry*, 59(16), 8886–8894. <https://doi.org/10.1021/jf201781z>
23
24
25 770 Huang, X., Dai, Y., Cai, J., Zhong, N., Xiao, H., McClements, D. J., & Hu, K. (2017).
26
27
28 771 Resveratrol encapsulation in core-shell biopolymer nanoparticles: Impact on
29
30
31 772 antioxidant and anticancer activities. *Food Hydrocolloids*, 64, 157–165.
32
33
34 773 <https://doi.org/10.1016/j.foodhyd.2016.10.029>
35
36 774 Joye, I. J., Davidov-Pardo, G., & McClements, D. J. (2015). Encapsulation of
37
38
39 775 resveratrol in biopolymer particles produced using liquid antisolvent precipitation.
40
41
42 776 Part 2: Stability and functionality. *Food Hydrocolloids*, 49, 127–134.
43
44
45 777 <https://doi.org/10.1016/j.foodhyd.2015.02.038>
46
47 778 Kelly, S. M., Jess, T. J., & Price, N. C. (2005). How to study proteins by circular
48
49
50 779 dichroism. *Biochimica et Biophysica Acta - Proteins and Proteomics*, 1751(2),
51
52
53 780 119–139. <https://doi.org/10.1016/j.bbapap.2005.06.005>
54
55
56 781 Kim, S., & Xu, J. (2008). Aggregate formation of zein and its structural inversion in
57
58
59 782 aqueous ethanol. *Journal of Cereal Science*, 47(1), 1–5.

- 1 783 <https://doi.org/10.1016/j.jcs.2007.08.004>
- 2
- 3 784 Lefèvre, T., Subirade, M., & Pézolet, M. (2005). Molecular description of the formation
- 4
- 5
- 6 785 and structure of plasticized globular protein films. *Biomacromolecules*, 6(6),
- 7
- 8
- 9 786 3209–3219. <https://doi.org/10.1021/bm050540u>
- 10
- 11 787 Liang, L., Tajmir-Riahi, H. A., & Subirade, M. (2008). Interaction of β -Lactoglobulin
- 12
- 13
- 14 788 with resveratrol and its biological implications. *Biomacromolecules*, 9(1), 50–56.
- 15
- 16
- 17 789 <https://doi.org/10.1021/bm700728k>
- 18
- 19
- 20 790 Mangavel, C., Barbot, J., Popineau, Y., & Guéguen, J. (2001). Evolution of wheat
- 21
- 22
- 23 791 gliadins conformation during film formation: A Fourier transform infrared study.
- 24
- 25 792 *Journal of Agricultural and Food Chemistry*, 49(2), 867–872.
- 26
- 27
- 28 793 <https://doi.org/10.1021/jf0009899>
- 29
- 30
- 31 794 McClements, D. J., & Gumus, C. E. (2016). Natural emulsifiers — Biosurfactants,
- 32
- 33
- 34 795 phospholipids, biopolymers, and colloidal particles: Molecular and
- 35
- 36 796 physicochemical basis of functional performance. *Advances in Colloid and*
- 37
- 38
- 39 797 *Interface Science*, 234, 3–26. <https://doi.org/10.1016/j.cis.2016.03.002>
- 40
- 41
- 42 798 Minekus, M., Alming, M., Alvito, P., Ballance, S., Bohn, T., Bourlieu, C., ...
- 43
- 44
- 45 799 Brodkorb, A. (2014). A standardised static in vitro digestion method suitable for
- 46
- 47
- 48 800 food-an international consensus. *Food and Function*, 5(6), 1113–1124.
- 49
- 50 801 <https://doi.org/10.1039/c3fo60702j>
- 51
- 52
- 53 802 Momany, F. A., Sessa, D. J., Lawton, J. W., Selling, G. W., Hamaker, S. A. H., &
- 54
- 55
- 56 803 Willett, J. L. (2006). Structural characterization of α -zein. *Journal of Agricultural*
- 57
- 58 804 *and Food Chemistry*, 54(2), 543–547. <https://doi.org/10.1021/jf058135h>
- 59
- 60
- 61
- 62
- 63
- 64
- 65

- 1 805 O’Sullivan, J., Arellano, M., Pichot, R., & Norton, I. (2014). The effect of ultrasound
2
3 806 treatment on the structural, physical and emulsifying properties of dairy proteins.
4
5
6 807 *Food Hydrocolloids*, 42, 386–396.
7
8
9 808 <https://doi.org/10.1016/J.FOODHYD.2014.05.011>
10
11 809 Paliwal, R., & Palakurthi, S. (2014). Zein in controlled drug delivery and tissue
12
13 810 engineering. *Journal of Controlled Release*, 189, 108–122.
14
15
16 811 <https://doi.org/10.1016/J.JCONREL.2014.06.036>
17
18
19 812 Patel, A., Hu, Y., Tiwari, J. K., & Velikov, K. P. (2010). Synthesis and characterisation
20
21 813 of zein-curcumin colloidal particles. *Soft Matter*, 6(24), 6192–6199.
22
23
24 814 <https://doi.org/10.1039/c0sm00800a>
25
26
27 815 Patel, A. R., Bouwens, E. C. M., & Velikov, K. P. (2010). Sodium caseinate stabilized
28
29 816 zein colloidal particles. *Journal of Agricultural and Food Chemistry*, 58(23),
30
31 817 12497–12503. <https://doi.org/10.1021/jf102959b>
32
33
34 818 Patel, A. R., & Velikov, K. P. (2014). Zein as a source of functional colloidal nano- and
35
36 819 microstructures. *Current Opinion in Colloid and Interface Science*, 19(5), 450–
37
38 820 458. <https://doi.org/10.1016/j.cocis.2014.08.001>
39
40
41 821 Penalva, R., Esparza, I., Larraneta, E., González-Navarro, C. J., Gamazo, C., & Irache,
42
43 822 J. M. (2015). Zein-Based Nanoparticles Improve the Oral Bioavailability of
44
45 823 Resveratrol and Its Anti-inflammatory Effects in a Mouse Model of Endotoxic
46
47 824 Shock. *Journal of Agricultural and Food Chemistry*, 63(23), 5603–5611.
48
49
50 825 <https://doi.org/10.1021/jf505694e>
51
52
53
54
55
56
57
58 826 Selling, G. W., Hamaker, S. A. H., & Sessa, D. J. (2007). Effect of solvent and
59
60
61
62
63
64
65

- 1 827 temperature on secondary and tertiary structure of zein by circular dichroism.
2
3 828 *Cereal Chemistry*, 84(3), 265–270. <https://doi.org/10.1094/CCHEM-84-3-0265>
4
5
6 829 Semenova, M. (2017). Protein–polysaccharide associative interactions in the design of
7
8
9 830 tailor-made colloidal particles. *Current Opinion in Colloid and Interface Science*,
10
11 831 28, 15–21. <https://doi.org/10.1016/j.cocis.2016.12.003>
12
13
14 832 Shukla, R., & Cheryan, M. (2001). Zein: The industrial protein from corn. *Industrial*
15
16 833 *Crops and Products*, 13(3), 171–192. <https://doi.org/10.1016/S0926->
17
18 834 6690(00)00064-9
19
20
21
22 835 Sobisch, T., & Lerche, D. (2008). Thickener performance traced by multisample
23
24
25 836 analytical centrifugation. *Colloids and Surfaces A: Physicochemical and*
26
27 837 *Engineering Aspects*, 331(1–2), 114–118.
28
29 838 <https://doi.org/10.1016/J.COLSURFA.2008.05.040>
30
31
32
33 839 Song, X., Zhou, C., Fu, F., Chen, Z., & Wu, Q. (2013). Effect of high-pressure
34
35 840 homogenization on particle size and film properties of soy protein isolate.
36
37 841 *Industrial Crops and Products*, 43(1), 538–544.
38
39 842 <https://doi.org/10.1016/j.indcrop.2012.08.005>
40
41
42
43 843 Sun, C., Dai, L., He, X., Liu, F., Yuan, F., & Gao, Y. (2016). Effect of heat treatment
44
45 844 on physical, structural, thermal and morphological characteristics of zein in
46
47 845 ethanol-water solution. *Food Hydrocolloids*, 58, 11–19.
48
49 846 <https://doi.org/10.1016/j.foodhyd.2016.02.014>
50
51
52
53 847 Sun, C., Dai, L., Liu, F., & Gao, Y. (2016). Simultaneous treatment of heat and high
54
55 848 pressure homogenization of zein in ethanol-water solution: Physical, structural,
56
57
58
59
60
61
62
63
64
65

1 849 thermal and morphological characteristics. *Innovative Food Science and*
2
3 850 *Emerging Technologies*, 34, 161–170. <https://doi.org/10.1016/j.ifset.2016.01.016>
4
5
6 851 Sun, C., Wei, Y., Li, R., Dai, L., & Gao, Y. (2017a). Quercetagenin-Loaded Zein-
7
8 852 Propylene Glycol Alginate Ternary Composite Particles Induced by Calcium Ions:
9
10 853 Structure Characterization and Formation Mechanism. *Journal of Agricultural*
11
12 854 *and Food Chemistry*, 65(19), 3934–3945.
13
14 855 <https://doi.org/10.1021/acs.jafc.7b00921>
15
16
17 856 Sun, C., Wei, Y., Li, R., Dai, L., & Gao, Y. (2017b). Quercetagenin-Loaded Zein-
18
19 857 Propylene Glycol Alginate Ternary Composite Particles Induced by Calcium Ions:
20
21 858 Structure Characterization and Formation Mechanism. *Journal of Agricultural*
22
23 859 *and Food Chemistry*, 65(19), 3934–3945.
24
25 860 <https://doi.org/10.1021/acs.jafc.7b00921>
26
27
28 861 Sun, C., Wei, Y., Li, R., Dai, L., & Gao, Y. (2017c). Quercetagenin-Loaded Zein-
29
30 862 Propylene Glycol Alginate Ternary Composite Particles Induced by Calcium Ions:
31
32 863 Structure Characterization and Formation Mechanism. *Journal of Agricultural*
33
34 864 *and Food Chemistry*, 65(19), 3934–3945.
35
36 865 <https://doi.org/10.1021/acs.jafc.7b00921>
37
38
39 866 Sun, C., Yang, J., Liu, F., Yang, W., Yuan, F., & Gao, Y. (2016). Effects of Dynamic
40
41 867 High-Pressure Microfluidization Treatment and the Presence of Quercetagenin on
42
43 868 the Physical, Structural, Thermal, and Morphological Characteristics of Zein
44
45 869 Nanoparticles. *Food and Bioprocess Technology*, 9(2), 320–330.
46
47 870 <https://doi.org/10.1007/s11947-015-1627-4>
48
49
50
51
52
53
54
55
56
57
58
59
60
61
62
63
64
65

- 1 871 Wei, Y., Sun, C., Dai, L., Zhan, X., & Gao, Y. (2018). Structure, physicochemical
2
3 872 stability and in vitro simulated gastrointestinal digestion properties of β -carotene
4
5
6 873 loaded zein-propylene glycol alginate composite nanoparticles fabricated by
7
8
9 874 emulsification-evaporation method. *Food Hydrocolloids*, 81, 149–158.
10
11 875 <https://doi.org/10.1016/j.foodhyd.2018.02.042>
12
13
14 876 Wei, Y., Yang, S., Zhang, L., Dai, L., Tai, K., Liu, J., ... Mackie, A. (2020). Fabrication,
15
16
17 877 characterization and in vitro digestion of food grade complex nanoparticles for co-
18
19
20 878 delivery of resveratrol and coenzyme Q10. *Food Hydrocolloids*, 105(17), 105791.
21
22 879 <https://doi.org/10.1016/J.FOODHYD.2020.105791>
23
24
25 880 Wei, Y., Yu, Z., Lin, K., Sun, C., Dai, L., Yang, S., ... Gao, Y. (2019). Fabrication and
26
27
28 881 characterization of resveratrol loaded zein-propylene glycol alginate-rhamnolipid
29
30
31 882 composite nanoparticles: Physicochemical stability, formation mechanism and in
32
33
34 883 vitro digestion. *Food Hydrocolloids*, 95, 336–348.
35
36 884 <https://doi.org/10.1016/j.foodhyd.2019.04.048>
37
38
39 885 Wei, Y., Yu, Z., Lin, K., Yang, S., Tai, K., Liu, J., ... Gao, Y. (2020). Fabrication,
40
41
42 886 Physicochemical Stability and Microstructure of Coenzyme Q10 Pickering
43
44
45 887 Emulsions Stabilized by Resveratrol Loaded Composite Nanoparticles. *Journal of*
46
47
48 888 *Agricultural and Food Chemistry*, 0(ja). <https://doi.org/10.1021/acs.jafc.9b06678>
49
50
51 889 Wei, Y., Zhang, L., Yu, Z., Lin, K., Yang, S., Dai, L., ... Gao, Y. (2019). Enhanced
52
53
54 890 stability, structural characterization and simulated gastrointestinal digestion of
55
56
57 891 coenzyme Q10 loaded ternary nanoparticles. *Food Hydrocolloids*, 94, 333–344.
58
59 892 <https://doi.org/10.1016/j.foodhyd.2019.03.024>
60

- 1 893 Yao, M., Xiao, H., & McClements, D. J. (2014). Delivery of Lipophilic Bioactives:
2
3 894 Assembly, Disassembly, and Reassembly of Lipid Nanoparticles. *Annual Review*
4
5
6 895 *of Food Science and Technology*, 5(1), 53–81. <https://doi.org/10.1146/annurev->
7
8
9 896 food-072913-100350
- 10
11 897 Ye, R., & Harte, F. (2014). High pressure homogenization to improve the stability of
12
13
14 898 casein-hydroxypropyl cellulose aqueous systems. *Food Hydrocolloids*, 35, 670–
15
16
17 899 677. <https://doi.org/10.1016/j.foodhyd.2013.08.022>
- 18
19
20 900 Zhang, B., Luo, Y., & Wang, Q. (2011). Effect of acid and base treatments on structural,
21
22
23 901 rheological, and antioxidant properties of α -zein. *Food Chemistry*, 124(1), 210–
24
25
26 902 220. <https://doi.org/10.1016/j.foodchem.2010.06.019>
- 27
28 903 Zhong, J., Tu, Y., Liu, W., Xu, Y., Liu, C., & Dun, R. (2014). Antigenicity and
29
30
31 904 conformational changes of β -lactoglobulin by dynamic high pressure
32
33
34 905 microfluidization combining with glycation treatment. *Journal of Dairy Science*,
35
36
37 906 97(8), 4695–4702. <https://doi.org/10.3168/jds.2013-7829>
- 38
39 907
40
41
42
43
44
45
46
47
48
49
50
51
52
53
54
55
56
57
58
59
60
61
62
63
64
65

Figure captions

Fig. 1 Effects of individual microfluidization pressure (A) and heating temperature (B) on the size and zeta-potential of curcumin loaded zein-PGA complex nanoparticles; effects of combined heating temperature and microfluidization pressure on the size and zeta-potential of individual and complex nanoparticles in the control group (C). (Different superscript letters (A, B, C...and a,b,c...) in the figure indicate significant differences ($p < 0.05$) in the particle size and zeta-potential)

Fig. 2 Impact of microfluidization pressure on the EE and LC of curcumin loaded in zein-PGA complex nanoparticles (A); impact of heating temperature on the EE and LC of curcumin loaded in zein-PGA complex nanoparticles (B); (Different superscript letters (A, B, C...) in the figure indicate significant differences ($p < 0.05$))

Fig. 3 Influence of microfluidization pressure on the physical stability of curcumin loaded zein-PGA complex nanoparticles (A); influence of heating temperature on the physical stability of curcumin loaded zein-PGA complex nanoparticles (B); the physical stability of the nanoparticles in the control group (C);

Fig. 4 Influence of microfluidization pressure (A) and heating temperature (B) on the photo stability of curcumin loaded in zein-PGA complex nanoparticles; the thermal stability of curcumin loaded in zein-PGA complex nanoparticles (C);

Fig. 5 Effects of thermal treatment, pH and ionic strength on the particle size (A, C and E) and zeta-potential (B, D and F) of curcumin loaded zein-PGA complex nanoparticles; (Different superscript letters (A, B, C...) in the figure indicate

significant differences ($p < 0.05$)

Fig. 6 Effect of different storage temperatures on the size (A) and zeta-potential (B) of curcumin loaded zein-PGA complex nanoparticles; the retention rate of curcumin loaded in zein-PGA complex nanoparticles at different storage temperatures (C); (Different superscript letters (A, B, C...) in the figure indicate significant differences ($p < 0.05$))

Fig. 7 Effects of microfluidization pressure (A) and heating temperature (B) on the fluorescence property of curcumin loaded zein-PGA complex nanoparticles; the fluorescence property of the nanoparticles in the control group (C);

Fig. 8 Circular dichroism of individual and complex nanoparticles in the control group (A); effects of microfluidization pressure (B) and heating temperature (C) on the circular dichroism of curcumin loaded zein-PGA complex nanoparticles;

Fig. 9 FTIR spectra of individual and complex nanoparticles in the control group (A); effects of microfluidization pressure (B) and heating temperature (C) on the FTIR spectra of zein-PGA complex nanoparticles;

Fig. 10 XRD spectra of individual component and nanoparticles in the control group (A); effects of microfluidization pressures (B) and heating temperatures (C) on the XRD spectra of zein-PGA complex nanoparticles;

Fig. 11 SEM images of curcumin loaded zein-PGA complex nanoparticles with and without individual microfluidization and heating or their combined treatments;

Fig. 12 The fluctuation in the mean size of curcumin loaded zein-PGA complex nanoparticles (A) and release **percentage** of curcumin in zein-PGA complex nanoparticles (B) during *in vitro* digestion; the bioaccessibility of curcumin loaded in different complex nanoparticles (C) and the morphology of different complex

nanoparticles during *in vitro* digestion (D). (Different superscript letters (A, B, C...)

in the figure indicate significant differences ($p < 0.05$))

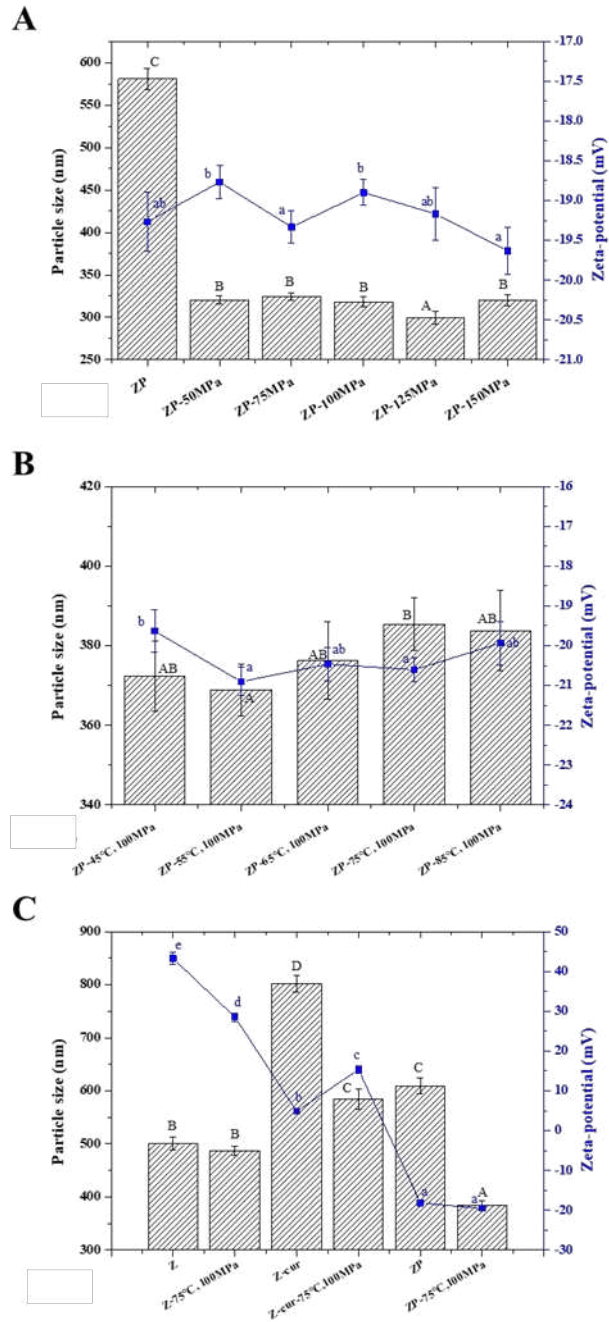


Fig. 1

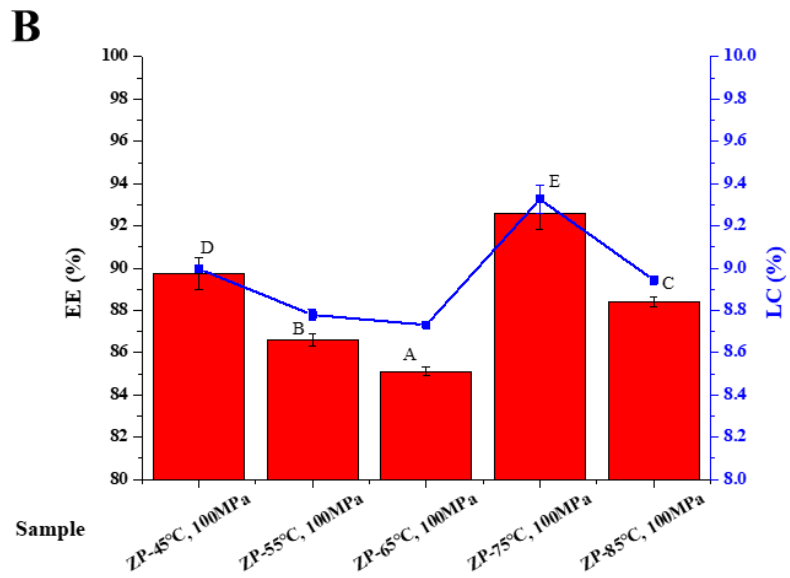
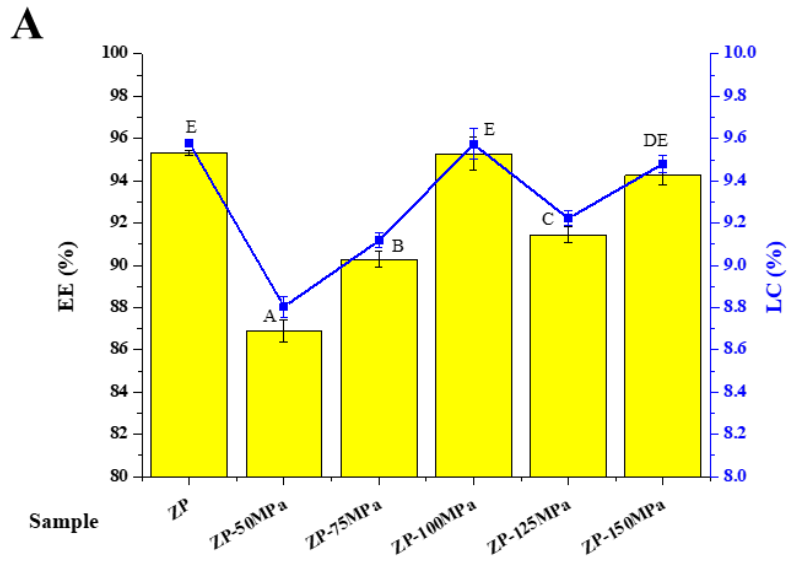


Fig. 2

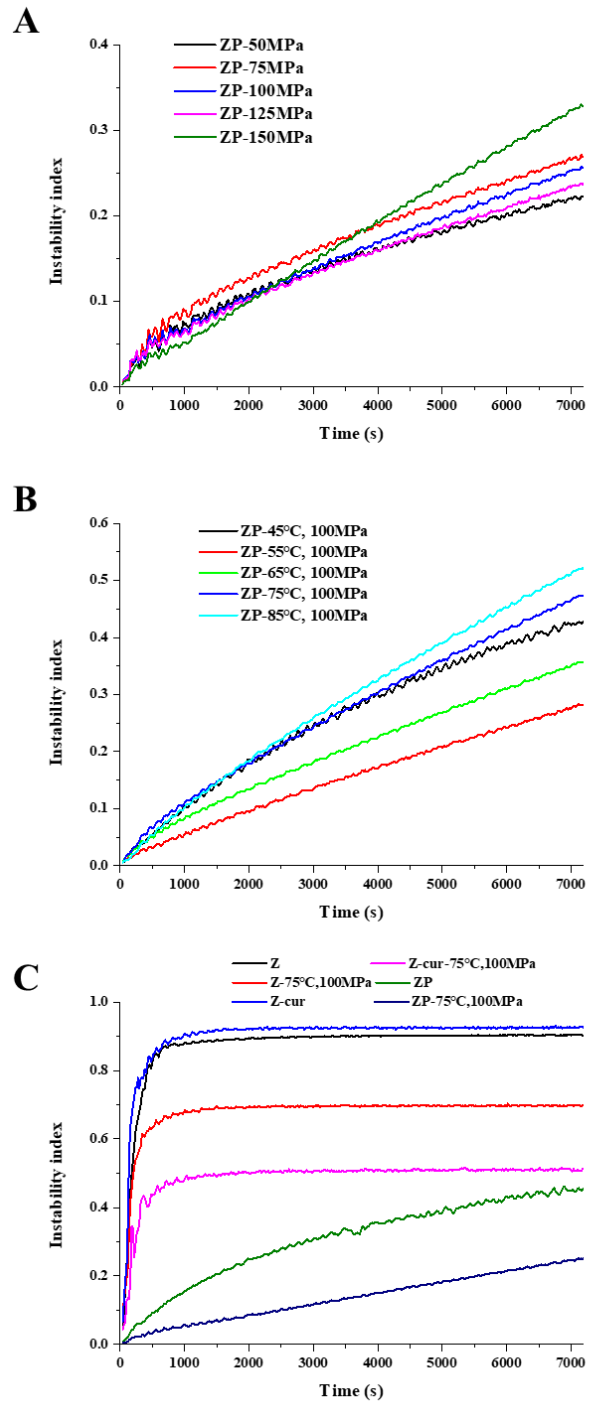


Fig. 3

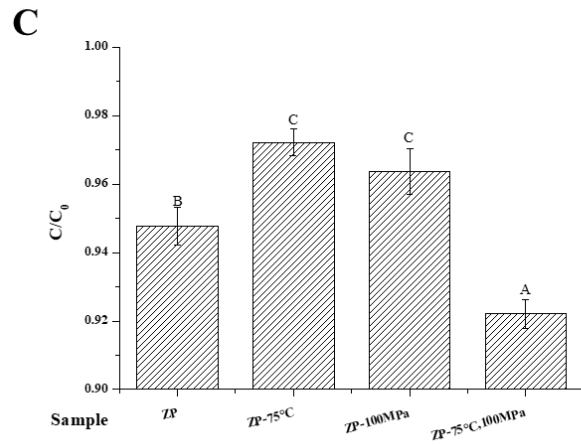
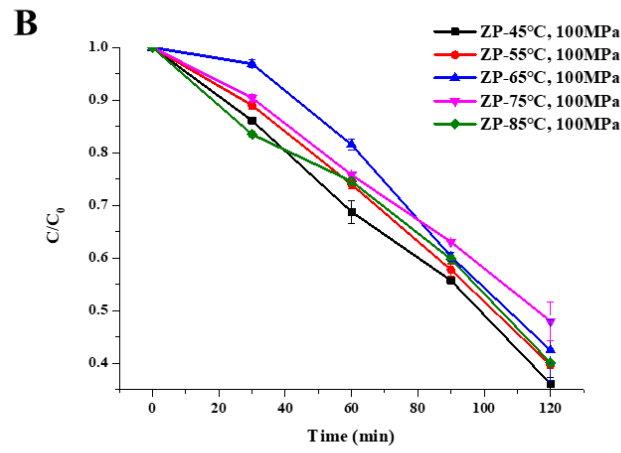
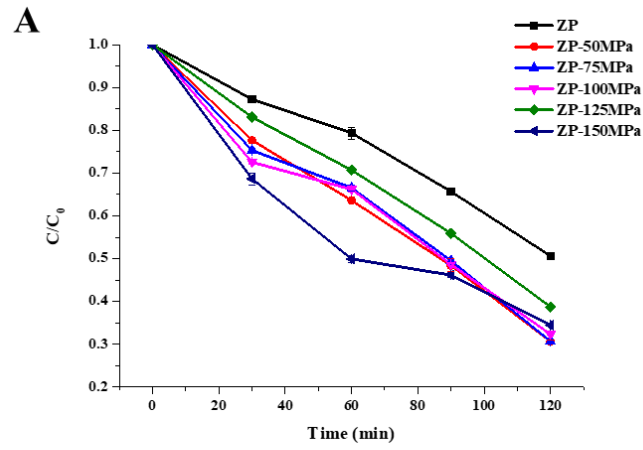


Fig. 4

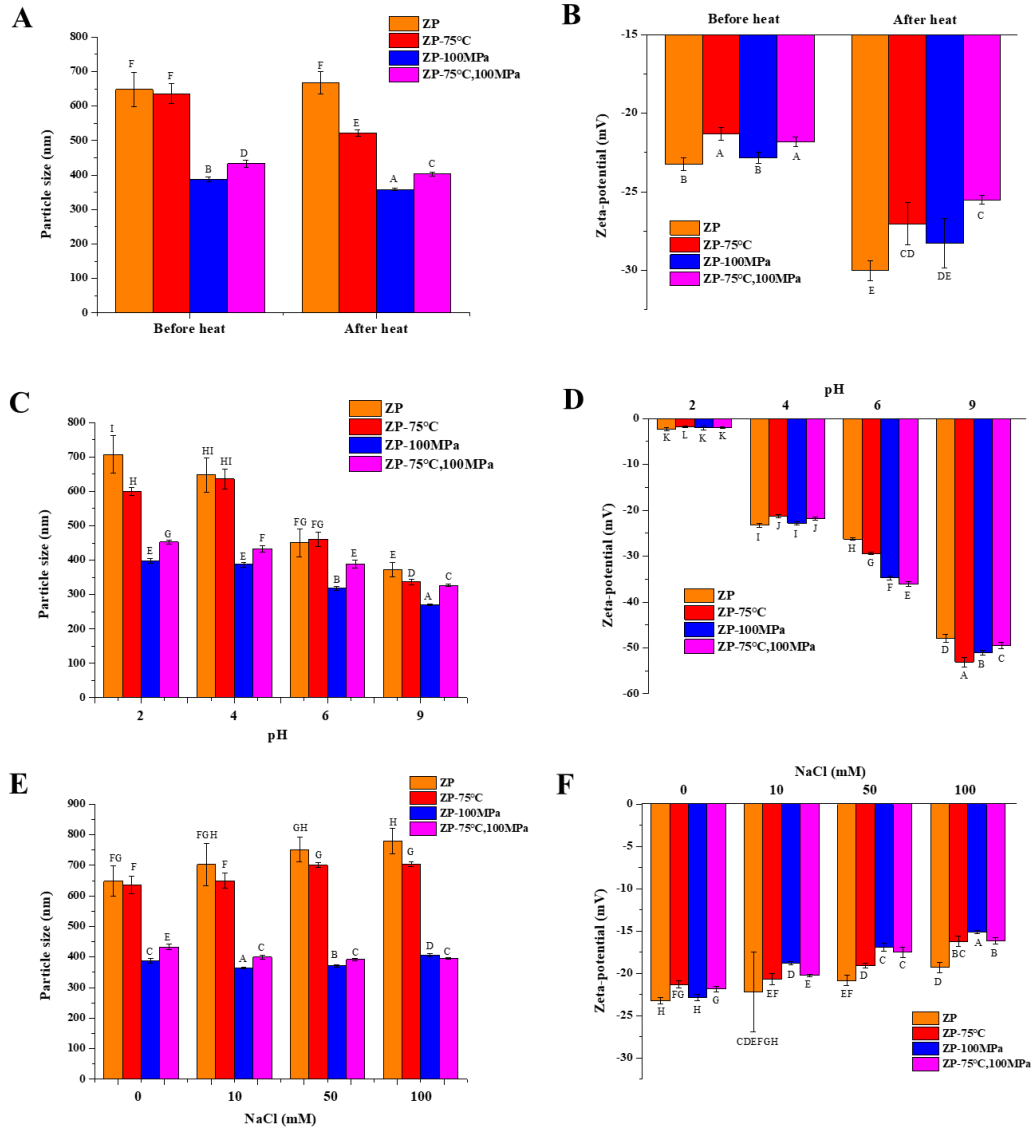


Fig. 5

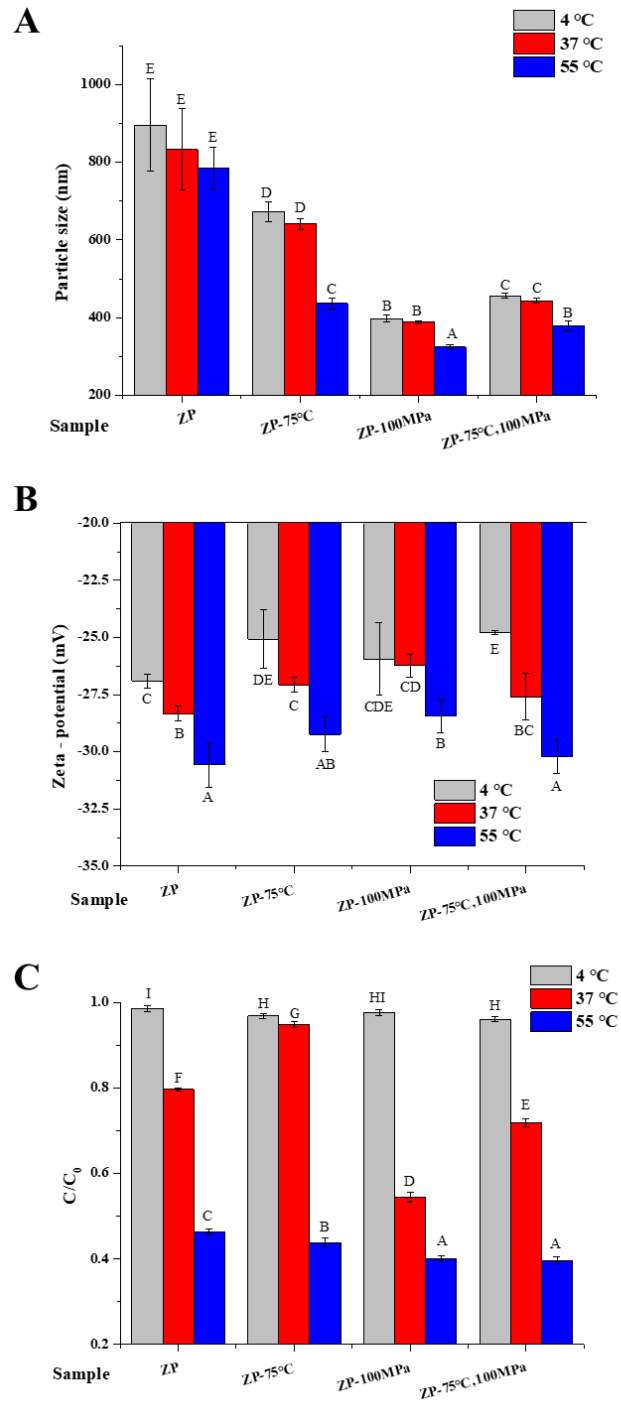


Fig. 6

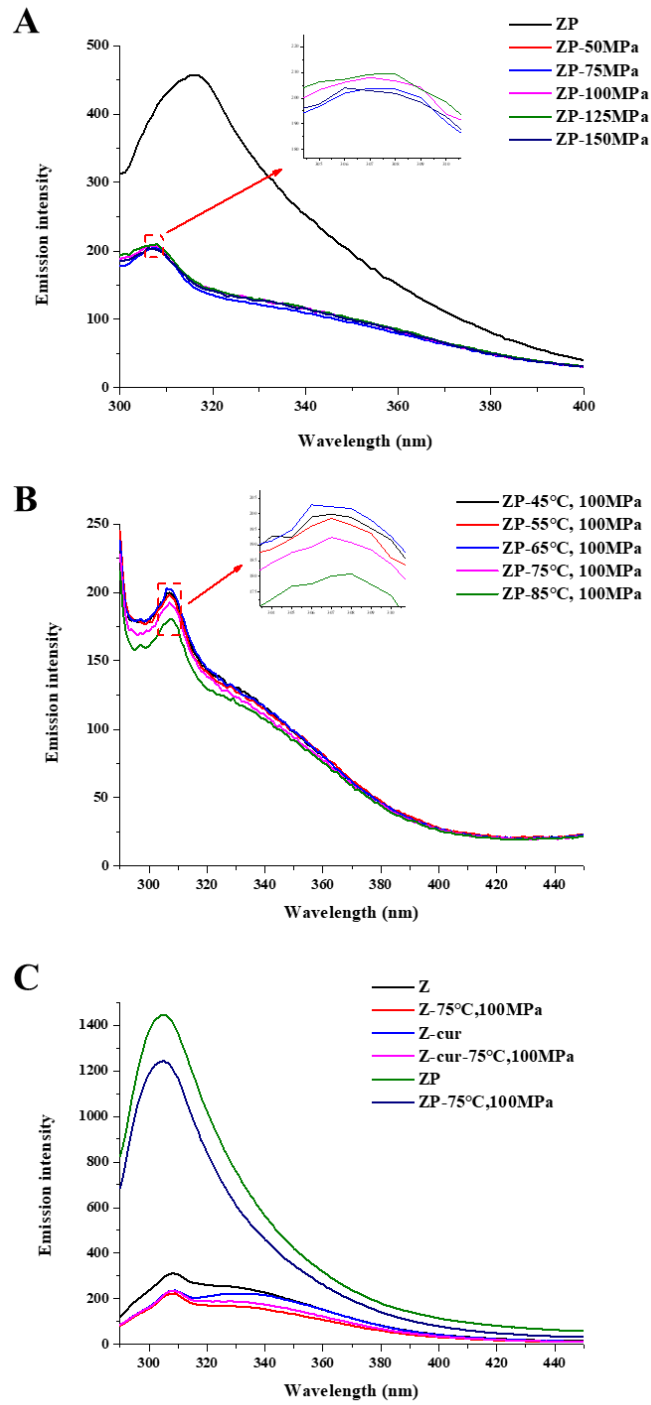


Fig. 7

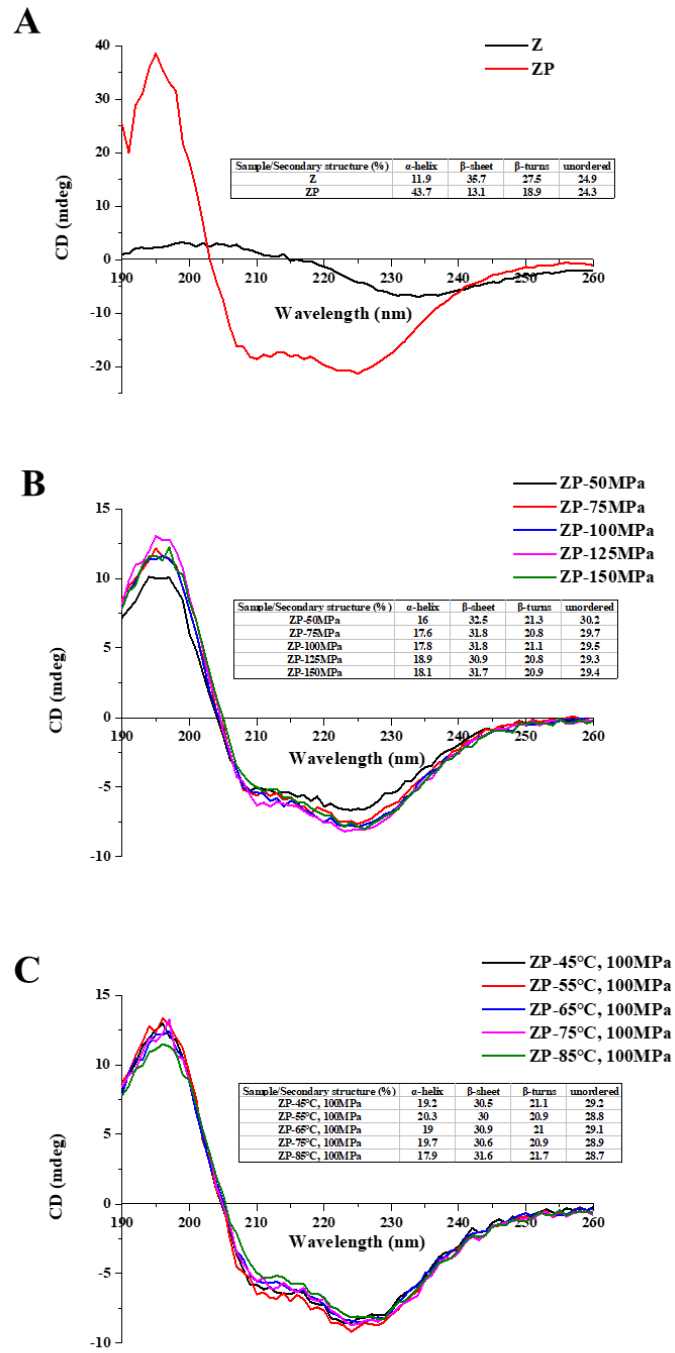


Fig. 8

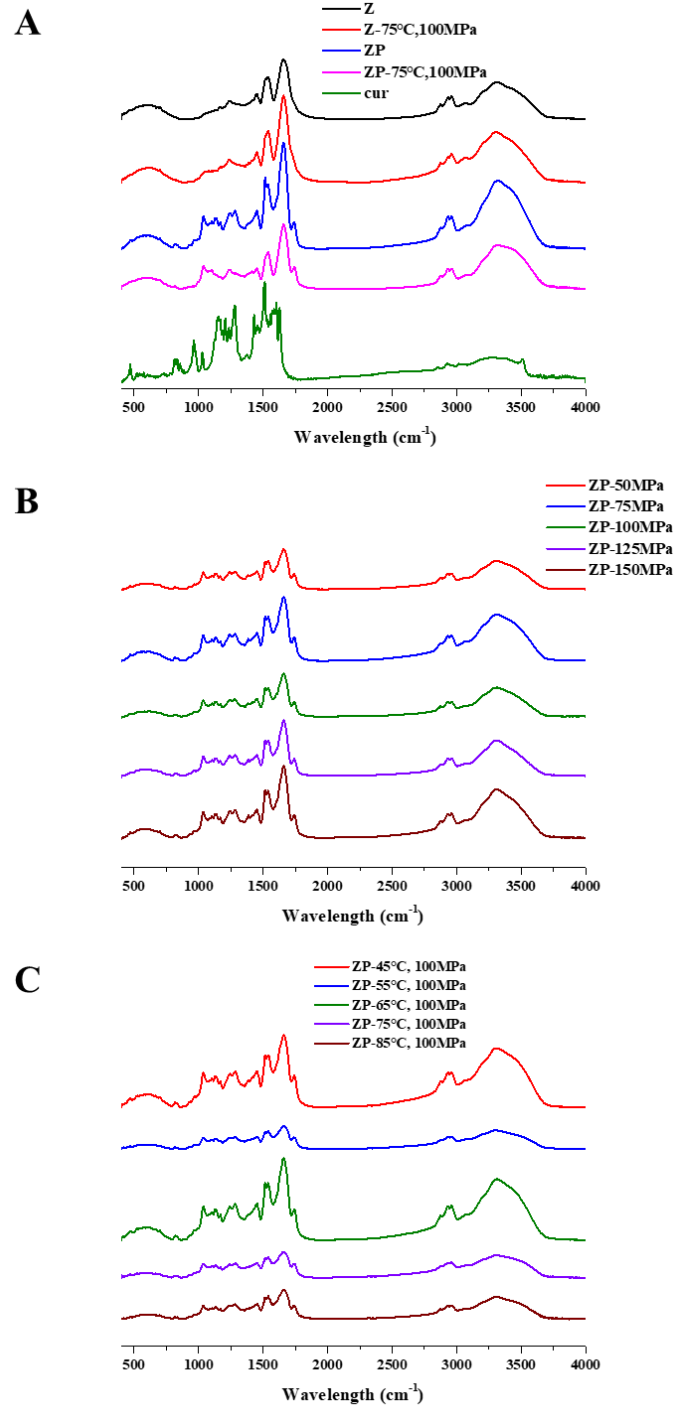


Fig. 9

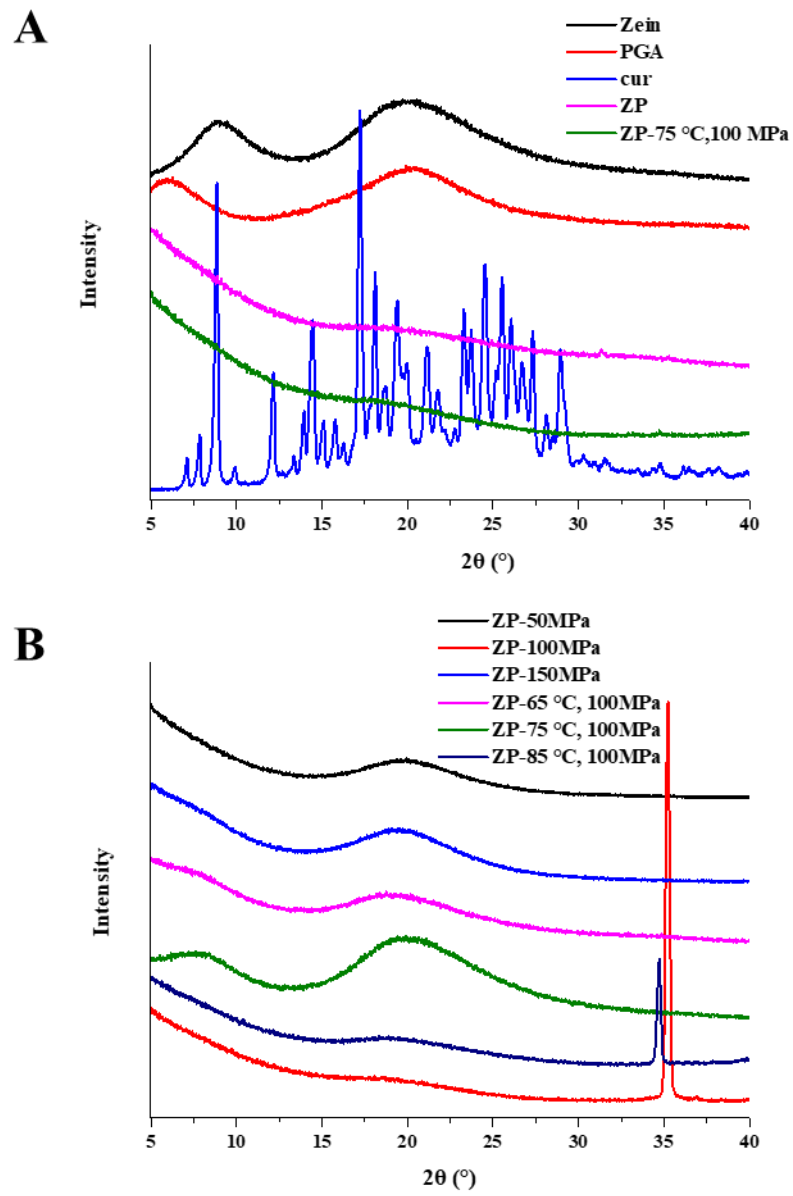


Fig. 10

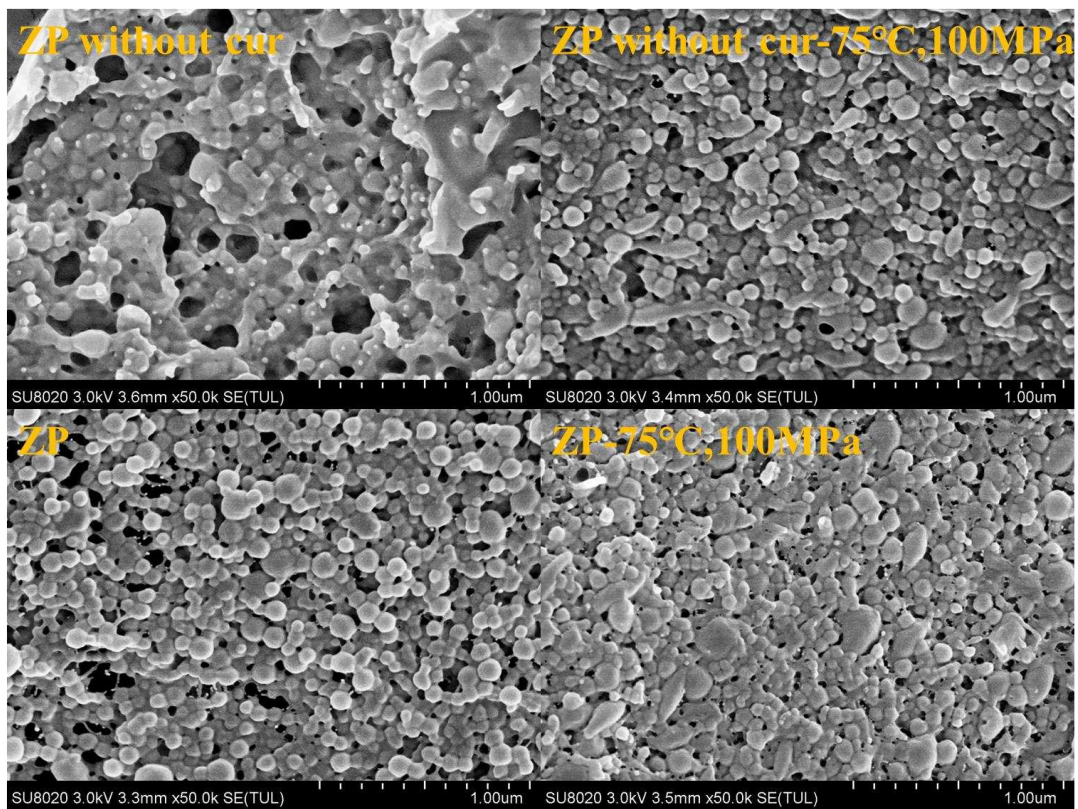


Fig. 11

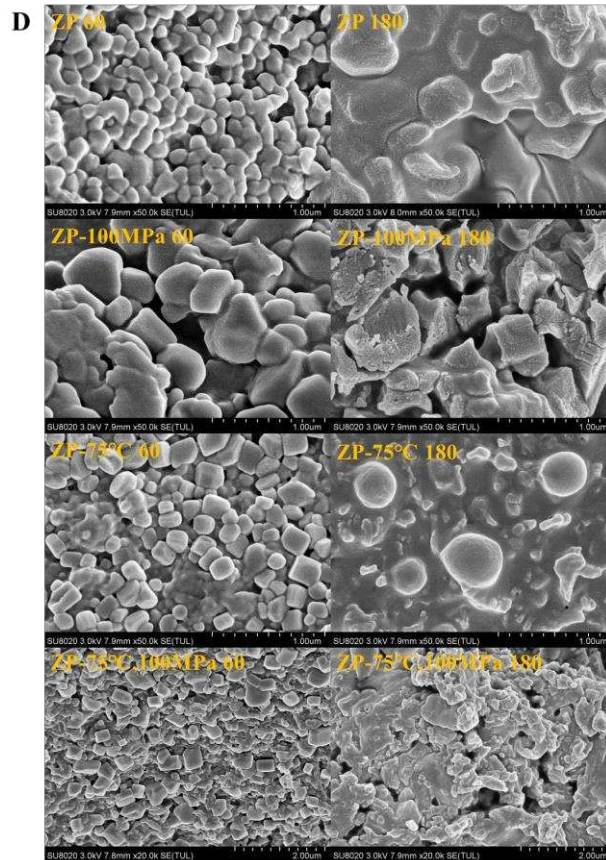
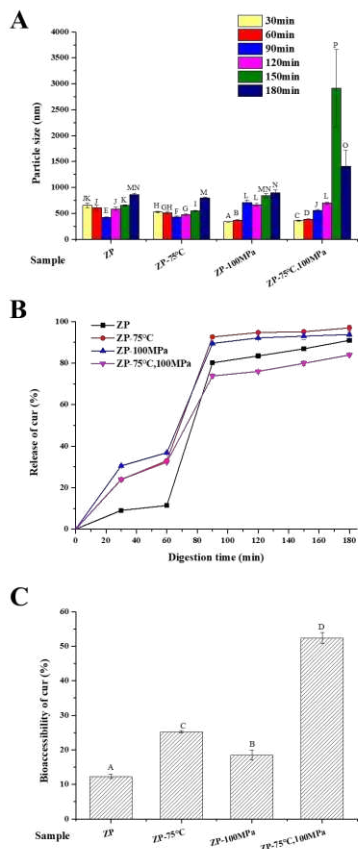
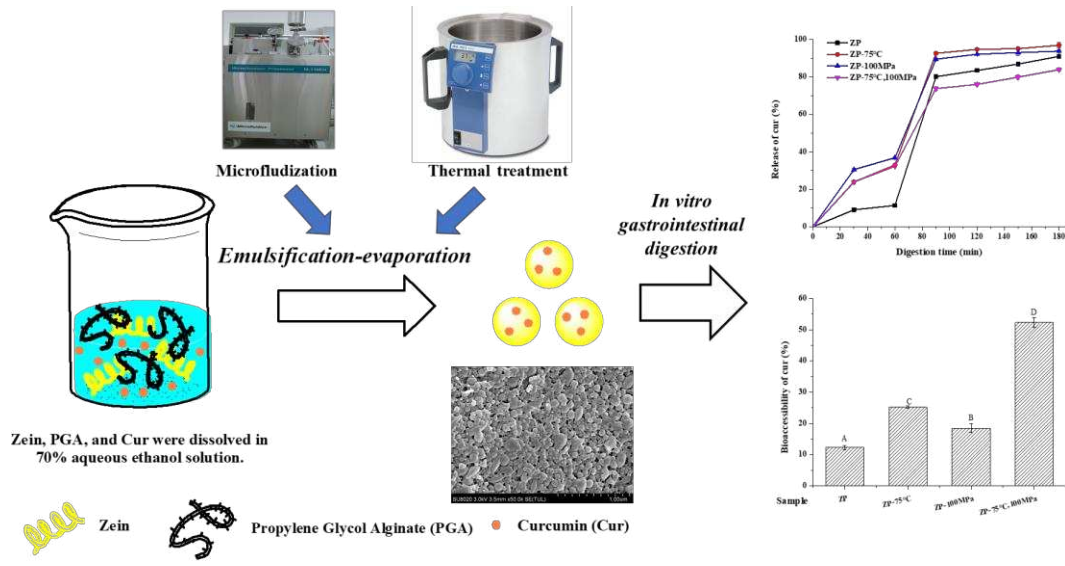


Fig. 12

Graphical abstract:



Author Contributions Statement:

Yang Wei: Conceptualization, Methodology, Software, Writing- Original draft preparation. **Chao Wang:** Data curation. **Xin Liu:** Software. **Alan Mackie:** Reviewing and Editing. **Liang Zhang:** Investigation. **Jinfang Liu:** Supervision. **Like Mao:** Software. **Fang Yuan:** Validation. **Yanxiang Gao:** Writing- Reviewing and Editing.

Conflict of Interest

The authors declare no competing financial interest in this study.